Deliverable 5.2: Final report

Prepared for:

New York State Energy Research and Development Authority

Albany, NY

and

The National Offshore Wind Research & Development Consortium

Albany, NY

Melanie Schultz
Program Manager

Prepared by:

GE Vernova Advanced Research

Niskayuna, NY

Project Manager 1: Sreekar Karnati,
Senior Engineer at GE Vernova Advanced Research

Project Manager 2: Jakcob Dean
Contract Administrator at GE Vernova Advanced Research

Technical Team: Ram Telikicherla, Bridget McShane, Gregory Dreifus, David Vanier, Mallikarjun Karadge, Patrick Shower (GE Vernova Advanced Research)

Sriram Praneeth Isanaka, Frank Liou (Missouri University of Science and technology)

NOWRDC Report Deliverable 5.2 NOWRDC Contract 180967 December 2024

Notice

This material is based upon work supported by the U.S. Department of Energy’s Office of Energy Efficiency and Renewable Energy (“EERE”) under the Wind Energy Technologies Office Award Number DE-EE0008390.

Table of Contents

Table of Figures

Acronyms and Abbreviations

ASTM	American Society for Testing and Materials
BS	British Standards
CMT	Cold Metal Transfer
CT	Computerized Tomography
DIN	Deutsches Institut für Normung
DNV	Det Norske Veritas
DNVGL	Det Norske Veritas Germanischer Lloyd
EDS	(X Ray) Energy Dispersive Spectroscopy
EPEN	Electrode Positive Electrode Negative
FEA	Finite Element Analysis
GB	Guojia Biaozhun
GE VAR	General Electric Vernova Advanced Research
GMAW	Gas Metal Arc Welding
HAZ	Heat Affected Zone
IEC	International Electrotechnical Commission
IIW	International Institute of Welding
IPM	Inches per Minute
ISO	International Organization for Standardization
LBW	Laser Beam Welding
LHW	Laser Hot Wire
MIG	Metal Inert Gas
MST	Missouri University of Science and Technology
NDE	Non-Destructive Evaluation
NDT	Non-Destructive Testing
NOWRDC	National Offshore Wind Research and Development Consortium
NY	New York
NYSERDA	New York State Energy Research and Development Authority
PMZ	Partially Melted Zone
PPE	Personal Protective Equipment
SEM	Scanning Electron Microscope
SW	Simufact Welding
TM	Thermo-Mechanical
USA	United States of America
UTS	Ultimate Tensile Strength
YS	Yield Strength

Executive Summary

This document provides a comprehensive overview of the efforts undertaken to develop a qualification requirement document for the welded assembly of cast iron components, along with a coupon-level testing plan for welded cast iron samples. The primary challenge addressed is the lack of established standards and design guides for the welded assembly of cast iron structural components. The project, led by GE Vernova Advanced Research in collaboration with DNV-GL and Missouri University of Science and Technology (MST), aims to establish performance and reliability metrics for assessing and qualifying welding processes for cast iron.

- Development of Qualification Requirements:

There are no clear set of standards or design guides for the welded assembly of cast iron components. Under this program through review of existing standards for welded structures and cast iron components, new requirement summary was drafted. A testing plan to analyze the mechanical properties and performance of welded cast iron samples was developed in collaboration with DNV and MST.

- Welding Process Optimization:

Laser-wire based welding and Metal inert gas welding were identified as joining technologies with high deposition productivity. These techniques were evaluated for feasibility of joining ductile cast iron. In the case of laser wire, cracking in the cast iron base material for weldments greater than 0.25" in thickness was observed. Through thermo-mechanical modeling and laser-based preheating to reduce thermal stresses, these issues may be managed. However additional work is required.

In the case of Gas Metal Arc Welding (GMAW), more consistent success across weldment designs and optimized parameters was observed. Successful procedures and parameters were established for single-material welds and a single multi-material weld (Double U Groove with Pure Nickel and Mild Steel). Welding process for 1" thick welds was scaled up to >2" thick welds, with hardware and process modifications. However, cracking was observed at intermediate thicknesses, aligning with simulated stress rise in thermos-mechanical studies.

- Characterization and Testing

Minimization of HAZ was a key trait for a successfully optimized weld. Additionally successful welds were also expected to be defect-free, particularly crack-free. Multiple candidate systems were tested, with NiFeMn-based welds selected for fatigue testing based on yield and ultimate

The program has made significant progress in developing a qualification requirement document and a coupon-level testing plan for welded cast iron components. Key findings include the successful optimization of GMAW processes and the identification of challenges in laser-wire based welding, particularly for thicker weldments. Thermo-mechanical modeling and mechanical characterization have provided valuable insights into the performance and reliability of the welds. Future efforts will focus on further optimizing the welding processes and addressing the challenges identified to ensure the successful implementation of welded cast iron components in large-scale applications.

1. Qualification Summary

Introduction

This program seeks to create, characterize, and optimize a method for the automated welded assembly of cast iron components, with the ideal eventual use case of large-scale cast components for offshore wind turbines. The proposed methodology for the production and assembly of such large-scale components is unique from the methods of single-piece casting or casting and bolted assembly currently in use today.

And while both casted components – uniform or bolted – and welded structures are accepted, understood, and standardized within many industrial fields, this specific combination is new to the industry. The unique nature of this method means it will require an amendment to existing standards and design guidelines. Current effort aims to develop procedures to qualify material and provide guidance to qualify these welded assemblies for use in the proposed application. In the case of cast components, the material properties, manufacture methods, and design recommendations are well understood and documented. Welded structures are a more varied area, highly dependent on the base material, welding material and method, human capabilities, environmental conditions, and overall structure to quantify the performance and strength. However, many standards and guidelines for the qualification requirements and quantification methods for welded steel structure are available.

The intersection of these two creates a gray area that must be explored for the method to be approved for wide-scale industrial use. The assurance of welded cast iron properties is impacted by the heat input from welding, requiring additional material characterization. The porosity of the base material as well as the presence of pores or gaps in the fusion zone must be investigated. The presence of any casting or welding defects must be assessed and avoided to ensure the strength and longevity of the weld joint. Each of these characteristics require specific testing methods, and for full qualification of the welded components the testing must be statistically relevant and clear in results.

The following will be a summary of the requirements needed for the qualification of welded cast iron assemblies, specifically assemblies produced with an automated welding process. Manual welding is limited in productivity and creates additional opportunities for variation and error, requiring additional review and potential rework. As such, this review is focused on automated weld processes only.

Standards Overview:

Certification of wind turbine technology is essential to ensure the turbine technology is appropriately engineered against damage for hazards and is resilient to function for the total design lifetime. Participating in certification processes provides validation that the wind turbine components, and systems have been designed, manufactured, and tested in compliance with the requirements as stated in the standards and certification schemes. Certification schemes such as IECRE-501 and DNV-SE-0441 series provide essential certification requirements for turbine system design, functioning, safety, and maintenance. These schemes include design load cases with methods, external conditions, design requirements, controls, mechanical systems, electrical systems, quality requirements, site assessment, assembly, site requirements and commissioning.

Standards such as IEC 61400-1:2019, DNVGL-ST-0361, DNVGL-ST-0126, DNV-RP-C203 provide relevant design requirements. For machinery structures made of welded steel DIN EN 1993-1-9, IIW-1823-07, DNV-RP-C203 can be considered as relevant Design Standards. These include information on,

- Relevant components of the wind turbine to be verified.
- Calculation requirements for different components under static, and fatigue loading, stability, and deflection analyses
- Relevant load cases to be considered during component design.
- Material and manufacturing process requirements to meet the specification and application requirement.
- Safety requirements for different components.
- Survival Probability requirements based on material capability and material variation
- Additional relevant guidance for different international standards.

these schemes and the certification process refers mainly to International Standards (ISO) and European Standards. National Standards (DIN, BS, ASTM, GB etc.) are only used in case International and European standards are not available. In the current effort to qualify welded assemblies of large castings, we need to consider not just standards overseeing cast structures (IEC 61400-8, DNVGL-ST-0361) but also incorporating welded structure codes and recommended practices (DIN EN 1993-1-9; DNVGL-ST-0126; DNVGL-RP-C203; IIW-1823-07).

IEC 61400-1:2019 lays out design load cases under situations such as power production, start-up, shutdown, emergency stop etc. and provides details on minimum loads. Calculations for limit state analyses such as ultimate and fatigue limit state with partial safety factors are provided in the standard. Material properties such as ultimate strength and fatigue life (S-N curve) are critical inputs to the design and certification process. For the essential static strength analysis, characteristic material properties are defined to have a 95% survival probability with a 95% confidence level. For the fatigue strength analysis of cast iron, S-N curves with at least 97.7% survival probability and a confidence level of 95% are used with a coefficient of variation less than 15%.For the fatigue strength analysis of welded structures, detail categories with 95% survival probability and 75% survival probability are required. However, welded structures do not include cast iron welds.

For fatigue strength analysis survival probability and confidence level are dependent on the applied design standard:

- DNV-ST-0361 survival probability 97,7% with a 95% cl (ym=1,25)
- DIN EN 1993-1-9 sp=95% cl=75%
- IIW-1823-07 95% with a cl=75%

Pleases note that cl=75% assumes always that the population is sufficient large to account for manufacturer and batch variation.

Please note that survival probabilities and confidence levels are connected to the safety factors e.g. in IEC 61400-8.

For setting up the qualification and certification process of cast iron welds, characteristic material capability information such as ultimate strength and fatigue life data need to be established and minimum specification requirements should be defined for weld qualification. This will require testing to generate the necessary basis data. Additionally, design recommendations, quality requirements such as factory acceptance criterion, and non-destructive evaluation will also need to be developed.

Testing Required for Qualification:

Qualification of the weld assembly process will involve multiple stages of exploration and qualification. These include, coupon level process exploration, testing at lab level and eventual scale up to production level. Initial evaluations will need to be performed to assess and identify candidate materials for welding process. Once successful processes have been identified, mechanical testing shall begin to establish characteristic material data. The different stages of mechanical testing for qualification are shown in Figure 1.

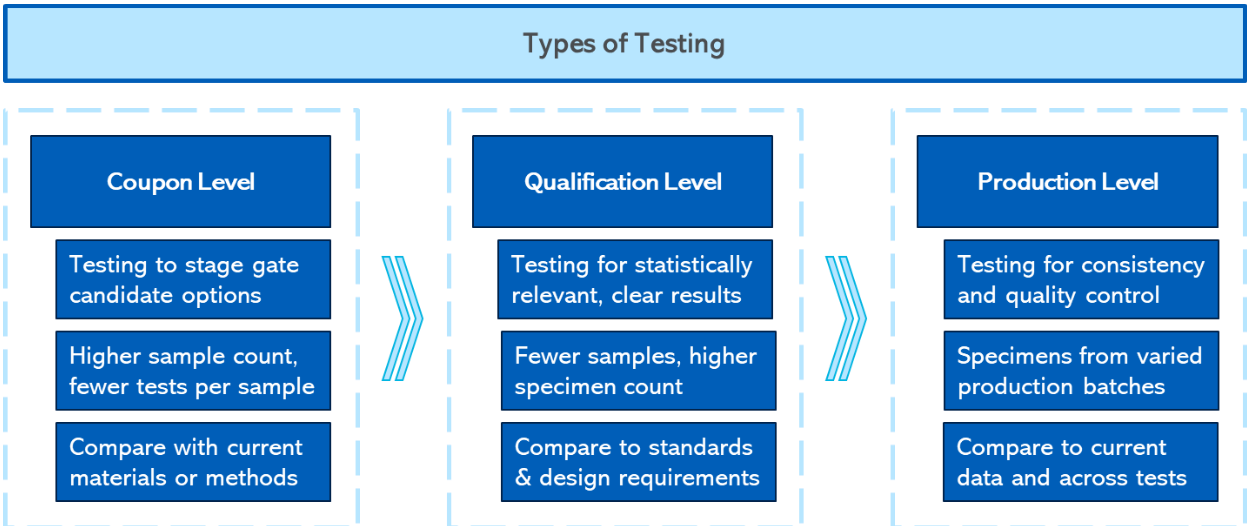

Figure 1: Chart depicting the progression of three levels of testing.

At coupon level testing, the objective of the evaluation is to stage gate candidate materials and processes and provide necessary screening information for down selection of promising methodology for joining. Follow on testing should be performed to generate basis data such as average ultimate strength data, lower knee point for fatigue or S-N curve with 50% survival probability (75% confidence level). At the qualification level, a much larger testing campaign should be performed to expand the testing population size for better statistical significance. At this stage necessary information for standard and certification incorporation. S-N curves for a 50% survival probability curve would be established at this stage considering a 75% confidence level. Companion testing of base material is warranted to realize compliance with standards, confirm the quality of the base material, and establish differences between cast iron base material and welded joints. Follow on testing will be at production qualification level. At this stage, testing should enable capturing variation from varied material sources, and production batches to improve the statistical significance and confidence levels. Laboratories conducting testing and analysis must be ISO 9001 certified and accredited according to ISO 17025.

Specific tests that would be conducted for a qualification-level testing procedure include:

Static Strength:

- Perform tensile testing according to, ASTM E8, ISO-6892-1
- Prepare tensile testing specimens according to the requirements in, ASTM E8, ISO-6892-1
- Testing equipment should be in accordance with the , ASTM E8, ISO-6892-1

Fatigue Strength:

- Perform fatigue testing according to ISO 1099 , ASTM E466 with satisfying requirements on testing equipment

- Prepare fatigue testing specimens according to the requirements in ISO 1099, ASTM E466. Specimens undergoing destructive testing, such as fatigue testing, should be inspected using NDT before and after extraction of the samples to ensure no pre-existing defects impact testing results

NDT (Ultrasound, Eddy Current ISO-17643):

- Preform NDT inspection according to,ISO 11666, ISO 17640,ISO 12680-3
- Prepare samples and specimens for NDT according to ISO 11666, ISO 17640, EN-12680-3inspection requirements

Fracture toughness and crack growth for metallic materials:

- Quasistatic fracture toughness ISO 12135:2021 , ASTM E399:23, ASTM E1820:24
- Fatigue crack growth method according to ISO 12108:2018, ASTM E647:24

Statistical Analysis

- Statistical analysis fatigue strength data according to ISO 12107.

Statistical analysis static strength data according to ISO 16269

Coupon Level Testing Plan

Coupon Type Descriptions:

This testing plan will cover the planned procedures and testing requirements for a coupon-level study of the proposed welding method and does not cover testing involved at production level. This will include the analysis and testing of candidate welds, down selected welds, and base material. The definitions for each are as follows:

Candidate welds: Distinct types of welds explored over the course of this effort. Welds can vary by base and weld filler material(s), bevel geometry, and welding method, not including the potential variation in welding parameters within a given method.

Down selected weld: A subset or single weld from the original candidate welds chosen based on weldability and weld performance for further production and testing.

Base material: The original material of the bevels and the material to be welded. In this case, EN 1563 ductile cast iron. The base material should comply with DIN-EN-1563. The base material shall be characterized for chemical, composition, microstructure, hardness, static strength (0.2% offset yield strength, ultimate strength, and impact testing to verify conformance with material specifications.

Down selection will be based on the weld quality and performance; visual analysis and observations while welding; metallography analysis of cross sections; and early mechanical testing, such as tensile testing.

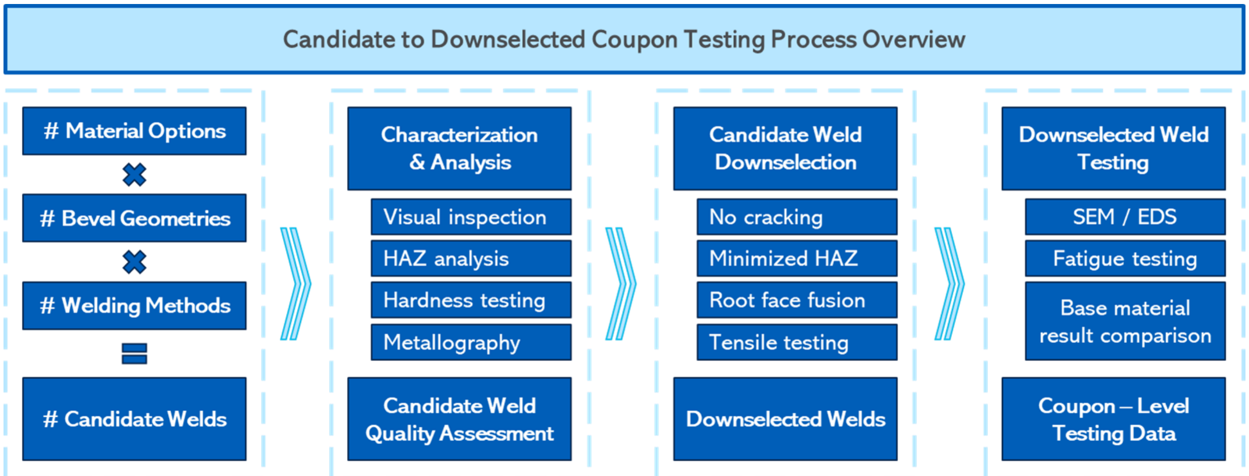

Figure 2: Chart depicting the process of candidate welds to down selected welds for coupon-level testing

Test Plan Breakdown:

This coupon-level testing plan includes a variety of testing and analysis methods, which have been sorted in two categories for the purpose of this discussion: characterization and mechanical testing.

Characterization: Tests and analysis meant to inform on the quality and internal structure of the material and welds, including microstructure analysis, hardness testing, and SEM.

Mechanical Testing: Tests meant to inform on the mechanical properties and performance of the material and welds, including tensile and low-cycle fatigue testing.

The coupon-level testing plan is summarized in the table below, noting the category of test, the test and collection method, and the test owner who will conduct the analysis. The weld coupons selected for these analyses will be assessed based on visual inspection. This visual inspection involves assessment based on presence of cracks, defects, bead quality which includes, continuity and physical dimensions. The tests in this plan are described further below the table. See Figure 3 for an illustrative representation of specimen collection from a welded sample.

Table 1: Down selection analysis and coupon-level testing plan summary for developing process parameters

Characterization and Testing Scope				
Test Type	**Test**	**Plan**	**Specimen Collection**	**Facility**
Characterization	**Optical Microscopy**	**1+ per shortlisted weld type** Shortlisting of candidate weld types occurs by visual inspection	Transverse sections	MST / GE VAR
	Vickers Hardness	**1+ per shortlisted weld** type based on SEM & Optical results	Transverse sections	MST / GE VAR

	SEM / EDS	**1+ per shortlisted weld type** Shortlisting of candidate weld types occurs by visual inspection	Transverse sections	MST / GE VAR
	NDT / NDE	**1 per down selected weld type**	Representative weld sections	MST / GE VAR
Mechanical	**Tensile**	**3 tests per candidate weld type** Tensile data used for down selection	Transverse cross-weld specimens	MST
	Fatigue	**25 tests per down selected weld type** 25 tests on base material	Transverse cross-weld specimens	MST

Characterization:

Optical Microscopy:

Metallography analysis of transverse weld sections cut from shortlisted welds, which are candidate welds that appear promising based on welding observations and visual inspection. Specimens must be within 2.5 cm in length and width. Equipment: Nikon Microscope Epiphot 200 or alike

SEM / EDS:

Scanning Electron Microscopy and X-Ray Energy Dispersive Spectroscopy will assess the microstructure and elemental composition across the weld region and HAZ using transverse sections of shortlisted welds. Specimens must be within 2.5 cm length and width and 6mm height. Equipment: Helios NanoLab 600 DualBeam or alike

Vickers Hardness:

Vickers Hardness tests will be used to gauge the hardness, and by proxy, brittleness, across the weld region and HAZ of the shortlisted welds. Specimens must be within 2.5 cm length, width, and height. Equipment: Struers Duramin – Digital Vickers/Knoop Hardness Tester or alike

NDT / NDE:

A non-destructive, internal method of analysis. During the process development stages, specific method is to be determined based on lab and equipment capability. Specimens and plates with defects observed may be excluded from testing if the defects are expected to be a consequence of controllable process steps. However, caution needs to be exercised to not skew the results through sample elimination or filtering. If defects are present and observed under NDT specimens will be excluded from future testing and necessary, process and material revisions should be made to address them. Separate and additional testing campaigns may be necessary to quantify the influence of defects, NDT could be used to catalog defects prior to testing and property data generation. During the qualification stages, bases plates shall be assessed according to EN12680-3. Such testing can be extended to specimen down selection for fatigue testing. MicroCT specimens must have a thickness or diameter within 6 mm in the area of investigation. Equipment: MicroCT: Xradia 620 or alike

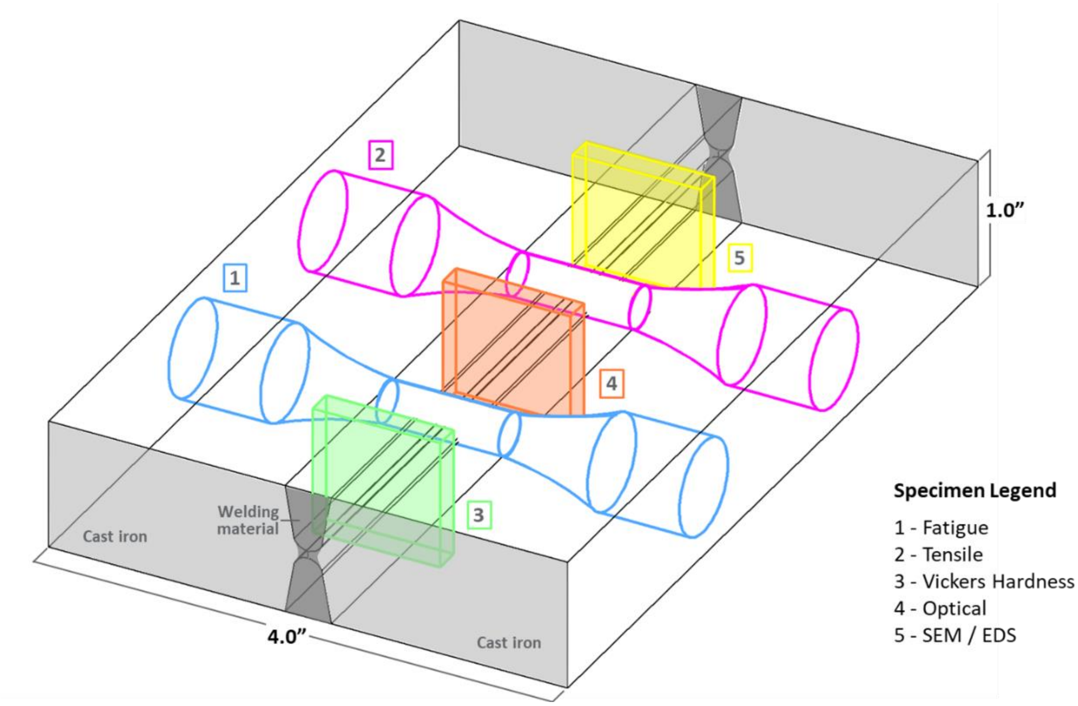

Figure 3: Specimen collection schematic for coupon-level testing, showing the placement of test specimens within weld samples. All specimens are centered along the width and height of the weld joint

Mechanical Testing:

Tensile Testing:

This test will be performed on shortlisted weld types and used to aid in the down selection of candidate welds. The test gauges the weld's response to tensile stress, a larger concern for the intended application compared to compressive stress. Specimens will be collected with the gauge length in the transverse direction of the welds, with the weld and root face centered within the gauge length. See Figure 4 for tensile specimen dimensions.

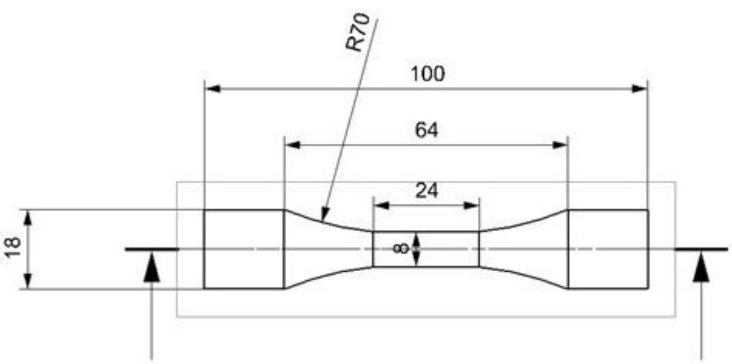

Figure 4: Fatigue and tensile testing specimen design

Fatigue Testing:

The cyclic fatigue test will gauge the weld's stiffness and strength response over repeated loading. This test will be performed only on the down selected weld type(s) and the baseline cast iron material, in accordance with the plan detailed below. The specimens will be collected in the same way as tensile specimens (see Figure 3), with a low-stress grind pass to minimize any irregularity or stress concentrations on the fatigue specimens. See Figure 4 for fatigue specimen dimensions. The fatigue test loading conditions will be informed by the results of tensile testing conducted on down selected welds. The frequency for the testing shall be observed and limited to avoid upheating of samples. The thickness of the gage section in this study captures the critical section such as the root pass, portion of weld-plate interface and the base material. However, the complete weld may not be captured due limitations of material thickness. For scaled up trials and larger thickness welds, large thicknesses of specimens (12mm and higher) are recommended.

The fatigue test will aim to determine 50% (mean) data only, building a fatigue curve of a minimum of 25 data points, or final specimen tests. The knee point, or fatigue limit, will be determined using a staircase testing method which will require a minimum of 15 specimens. The next 10 to 15 specimens will use a Pearl string distribution to find the slope of the fatigue curve. Separate test campaigns to gather fatigue data at R=-1 and R=0 (the ratio of minimum stress divided by maximum stress) are recommended along the knee point. Run out limit shall be defined with N=1e7 cycles for the limited fatigue lifeline. See Figure 5 for an illustration of the two specimen groups – the Pearl string distribution assessing the 50% data in red, and the staircase testing for the fatigue limit in blue.

Other topics of note for the coupon-level testing plan include the management of specimens and samples, and the collection and organization of testing data. See below for expectations on these topics.

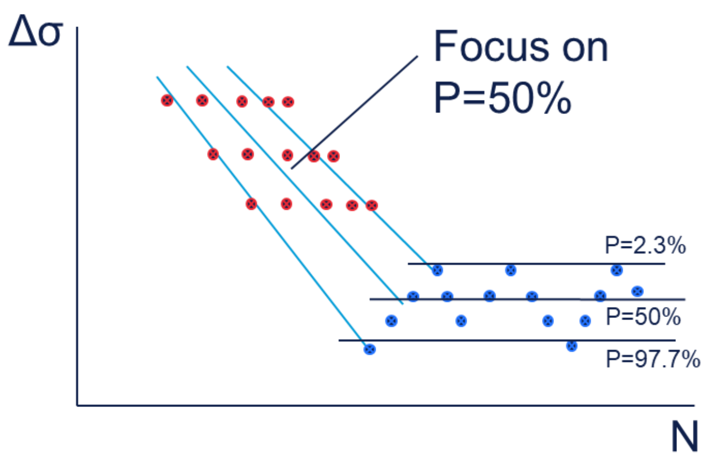

Figure 5: Illustration of stress level distribution for coupon-level fatigue test

Specimen Management:

Specimen Preparation: Weld samples will be shipped and stored post-welding in such a way to minimize rusting, which are prone to rust. When samples are to be cut or otherwise machined into specimens for analysis or testing, they will be cleaned with isopropyl alcohol and a wire brush to remove any rust present, and then prepared as necessary for the test.

Specimen Labeling: Weld samples will be labeled to allow for easy reference to a spreadsheet or other notation method tracking the relevant weld information – filler material(s), weld method, bevel type, and any relevant welding parameters, such as weld settings or passes used to fill the bevel volume. Specimens will be labeled in such a way to refer to the weld sample they were machined from, whether by a related name (ex: Sample Name_1,2, etc.) or with a new label and notation in a spreadsheet linking the specimen to the sample.

Specimen Storage: Specimens should be stored in such a way to minimize oxidation and any potential for damage. Specimens should be labeled with their name and test date, and stored for the length of the program or until permission to dispose of them is granted.

Data Collection and Reporting:

Test data collection: Test data should be clearly named or labeled with the specimen's name and date, and all data should be well organized within a single folder or sub-folder location.

Final data collection and report: Test data will be summarized into a clear set of findings or recommendations regarding weld quality, in the case of testing and analysis used for candidate and shortlist weld down selection. Testing and analysis of down selected welds and base material should be summarized into plots, charts, or tables to present clear results or findings for the weld(s) and base material, including comparisons when relevant.

2. Welding process development

LHW Welding Process Optimization

Use of LBW potentially provides greater control over the energy input and distribution required to perform a weld, a benefit when working with a material like cast iron, which is prone to embrittlement under heating and rapid cooling. This modality, used in combination with hot wire feeding (HW), is expected to create a much smaller melt pool and reduce heat affected zone in the weld. Hot wire feeding is a process where the feed wire is resistively heated to elevate its temperature prior to melting. This wire preheating reduces the overall energy needed to maintain a melt pool, therefore reducing the heat affected zone around the weld.

The LBW Optimization process focused primarily on the development of a standardized weld fixturing and weld path process, and experimentation within key welding variables. The welds were first cleaned to remove contaminants and rust from the weldment surface. Once the weld surface is prepared, the weldments are placed within a custom fixture which secures the weldments in place and leveled while still allowing the flow of shield gas from above and below the weld. The fixture is designed to allow easy removal and replacement of the weldments into the same orientation and location, such that the weld path is in the same orientation throughout the welding process even when the weldment is being removed, flipped, and replaced during balance welding.

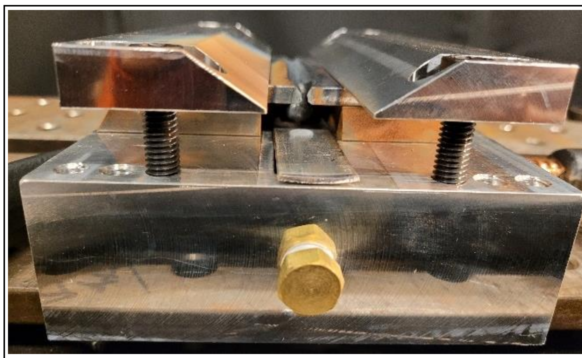

Figure 6: Weldment Fixturing

Figure 7: Wire Feed Alignment

Figure 8: Root Pass(es)

Figure 9: Fill Passes

Once the weldment is secured into the fixture, the welding operator ensures that the planned weld path is colinear with the centerline of the weldment pieces and aligns the wire feed to the just above the bevel, in line with the laser path. Once the fixturing and alignment checks are complete, the welding operators ensures that the proper safety equipment and PPE are engaged and in-use and begins the weld.

The first weld pass is a root pass located at the base of the bevel(s), creating the initial joint of the two sides (left, right) of the weldment. In the case of double bevels, this landing is between the upper and lower bevels, halfway through the weld height, and must be completed twice – one root pass depositing material in the upper bevel before the weldment is removed, flipped over, and replaced to deposit a second root pass in the lower bevel. This alternate welding process is termed balanced welding and was implemented to manage residual stresses and mitigate distortion. This remove-flip-replace process must be completed between every layer of weld passes during balance welding, to ensure even thermal input to the upper and lower bevels by alternating the sides being welded. As such, after the second root pass, the weldment is again flipped to upper bevel for the first fill pass, and the process repeats until both bevels are entirely filled and the welding is complete.

Within this welding procedure, a host of variables can be adjusted both weld-to-weld and pass-to-pass. The key variables for the optimization of laser beam welding of cast iron are shown in the table below, summarizing the range of process parameters used successfully in cladding and welding trials.

LHW Trials: Key Welding Parameters Varied During Optimization *Wobbler conditions maintained throughout cast iron optimization trials*					
Fill Material	**Travel Speed**	**Wire Feed**	**Laser Power**	**Hotwire**	**Wobbler**
• 3 Nickel-based contacting materials • Mild Steel non-contacting weld fill for multi-material welds	• 7 – 13 IPM	• 70 – 120 IPM	• 1600 – 5000 W	• 300 - 1100 W	• Frequency: 200 Hz • Amplitude: 2.0 mm

When tuning the weld parameters and adapting weld conditions, defects and failures are often more informative than successes, as they help eliminate unsuccessful parameter conditions and combinations. Common signs of unsuccessful welds and the associated process parameters that can exacerbate or alleviate these conditions are noted below.

- Balling: Irregular surface of the cladding or weld pass often rounded and raised portions. Largely caused by an incompatible pairing of wire feed rate, travel speed and power for the given base and welding material. This phenomenon is indicative of insufficient of energy input.

- Arcing: Electric arc formation between the feed wire and base material when electric contact is broken, and a gap is created. Irregular surface of the cladding or weld pass often misaligned or raised "layers" of the weld material along the weld bead led to inconsistent contact and gap creation between the weld wire and base piece. Additional cause likely due to a lack of stable wire melt along bead, leading to the inconsistent hot wire contact with the weld, voltage and arcing between the melt pool and feed wire.
- Lack of penetration: Lack of and/or irregular depth of the melt pool leading to insufficient melting of landing. Energy and power need to be adjusted to create sufficient melting and depth of penetration.
- Cracking: Cracking can occur due to the failure of material under stresses created during or after the weld process. Cracking can occur in both the welding (filler) material or the base material itself – cracking in the base material indicates that the welding parameters are not only unsuccessful for welding but actively damaging to the base material. As with any of the weld related defects, the cause is likely to be an issue of the material(s) ability to withstand the thermal energy input over time, creating stresses as the material heats and cools.

Figure 10: Cladding passes showing examples of balling and arcing – see the irregular surface of the weld

Figure 11: Cladding passes showing misalignment of wire feed – see wire portions that had fallen into to the weld pool

Figure 12: Welding pass showing cracking in the base material – see the crack line running along right edge of filler material

If observed in any of the cladding or welding trials attempted, these welding flaws were noted with the specific parameters used to create the weld, and the parameter set would be iterated and trialed again to attempt to eliminate these issues. The most successful parameters were used when moving from LHW cladding to welding of actual bevels, which saw varied success and failure over the welding materials and bevel designs available for trial.

While automated LHW welding offers potential for finer tuning of welding parameters and a minimized HAZ, it is not an established process for use with cast iron and requires more significant learning and optimization compared to the more traditionally used GMAW method. In this program, LBW and LHW welding trials have been conducted to initiate and optimize laser welding of cast iron weldments. Thus far, only small-scale welds (under 0.25” in thickness) have been made successfully with no cracking. Trials with both Pure Ni and a Nickel-Chrome alloy have been attempted and while the root pass and some fill passes have been deposited successfully, subsequent passes cause cracking in the cast iron.

Cracking in the cast iron is of particular concern as it could indicate that the thermal load of the welding process or the rate of heating or cooling is too large for the cast iron to undergo without embrittlement and subsequent cracking. The key thermal parameters (laser power, hot wire voltage) were manipulated to reduce the thermal load as much as possible while maintaining a consistent melt pool and material fusion, but the cracking persisted when thicker weldments were used, and more passes were required. The residual stresses where significant enough to cause cracking in the heat affected zone.

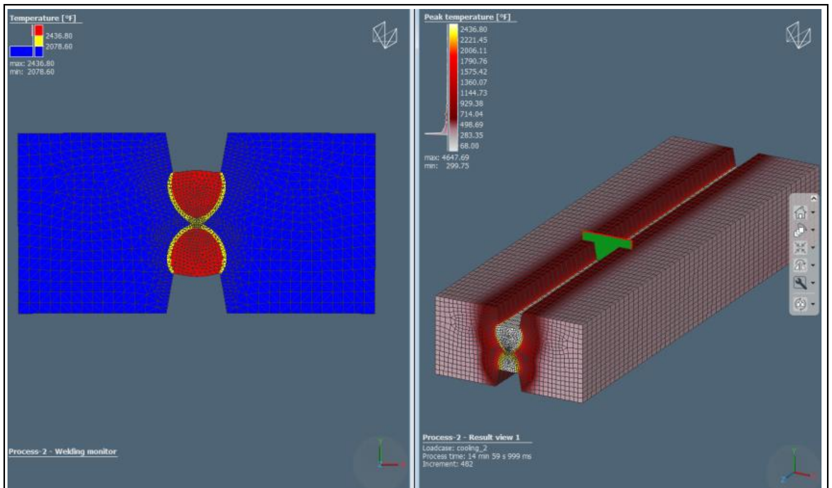

Figure 13: Example of thermo-mechanical simulation for a weld

Thermo-mechanical modeling of the weld will be particularly useful to understanding the development of stresses during welding, as it will allow simulation of various welding conditions and LBW / LHW parameters to better understand and potentially alleviate this cracking issue. It is possible that the potential successful welding conditions and parameters for successful cast iron LHW welding will be found using thermo-mechanical modeling and can be validated and further optimized with physical LHW welding.

Another potential pathway to successful LHW welding of cast iron is through preheating – a technique that has been traditionally employed for welding of cast iron to prevent the rapid heating and cooling that causes embrittlement. Traditional preheating techniques have not yet been explored as they are unrealistic for the scale of components this program aims to develop welding techniques for. However, laser-based preheating is an area of potentially future exploration as it could mitigate some of the thermal load concerns without adding the equipment, fixturing, and scaling complications that preheating of large (>10 ft) components could entail.

MIG Welding Process Optimization

The MIG welding process also referred to as GMAW – or Gas Metal Arc Welding – was selected as the best candidate for the welding of cast iron. MIG welding of cast iron entails the same struggles to manage the HAZ and thermal stresses on cast iron, without the hot-wire modality to minimize direct energy input. However, there are alternative mechanisms which can reduce the heat input during welding; Fronius International's Cold Metal Transfer (CMT) technology uses wave form power input in addition to short circuiting as a mode of material transfer for efficient heat management. The alternating Electrode Positive and Electrode Negative (EPEN) controls the localized heat of the arc and reduces the energy and temperature needed to maintain a melt pool. This reduces the temperature and therefore HAZ in the base metal, resulting in less brittle material.

Four categories of weld candidates were explored, based on the weldment geometry – Double U Grooves vs. Double V Bevels – and the number of materials – single material, using only a nickel-based contacting weld filler, and double material, using a nickel-based material to coat the weldment and mild steel mild steel weld filler to complete the weld. Within each category, at least one weld for each of the three contacting materials would be trialed.

The following subsections summarize the welding process and learnings for each category.

Single Material, Double V Bevel: The V shape of the bevel providing simpler machining of the weldments and easier access to the weld base than other, narrower bevel geometries. However, the angle of the bevel means that with each addition inch of weldment height or layer of weld passes required, the amount (and cost) of weld material added raises exponentially rather than linearly. Without a secondary, more common, and lower-priced weld filler material to fill the bulk of the bevel volume, this weld design becomes high in cost relatively quickly as the bevel size increases.

Additionally, the wide nature of the bevel at larger weldment heights creates additional potential stress points in the weld – as more passes are required to deposit a layer of material, and there is more thermal energy input into a relatively concentrated area in short succession, and each additional bead deposited creates a new boundary along which defects like cracks, voids, or pores, could form.

No cracks or prominent defects were observed in the 3 single material, Double V Bevel welds created during the optimization process, but additional adjustment of the process parameters was required as the width increased in later passes – three or more parameter sets might be used for the V Bevel compared to the two sets used in U Groove welds. Moreover, the higher potential for defects and higher cost of the weld is of note for the 3 - 4” weld heights required for this program and will be considered as a factor during downselection.

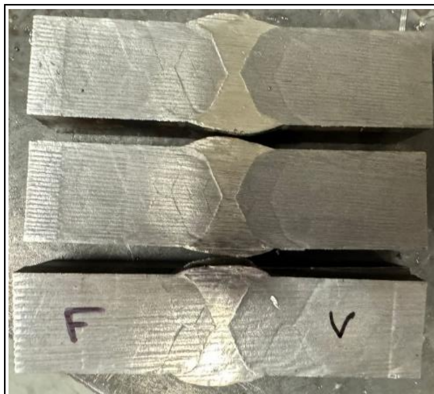

Figure 14: Cross sections from Single Material, Double V Bevel Weld Sample

Single Material, Double U Groove: In comparison to the single material, double V bevel, this weld is more material and cost efficient, with a less angled bevel shaped that maintains a more consistent width across the weldment height. This relative consistency in dimension allows for consistency in welding passes per layer. This also lowers the cost per weld, especially at large scales, as the cross-sectional area is much less than that of a V bevel of the same height.

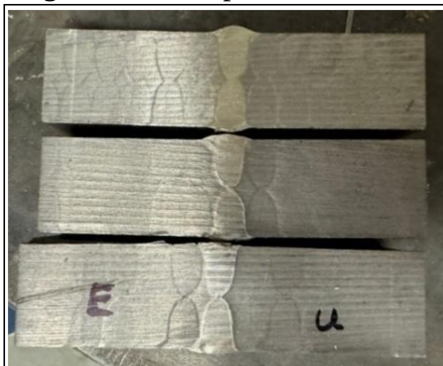

Figure 15: Cross sections from Single Material, Double U Groove Weld Sample

These welds were successful across all three materials. First, the key parameters (power, speed) were trialed and iterated for the filler materials through bead on plate experiments. Later these parameters were adjusted as needed between root passes and fill/cap passes.

Double Material, Double U Groove: In the case of double material welds, the process complexity and number of parameter sets used is increased, compared to their single-material counterparts, but the cost efficiency of this weld type adds appeal for large-scale use cases. The final optimized process for this weld category has been included in detail below for the sake of illustration, as it is more in depth than the simpler fixturing – root pass – fill pass process used in both the LBW and MIG single material welds and shown in Figure 6 through Figure 9.

The first step is to individually coat both halves (left, right) of the weldment in the nickel-based contacting material, prior to any joining welds/passes are made (Figure 16**Error! Reference source not found.**- Figure 19). This ensures that the secondary filler material will only contact the nickel-based passes rather than the cast iron itself. After the faces of the bevels have been fully covered, an additional nickel pass is added to recreate the "landing" of the bevel (Figure 19- *Figure 21***Error! Reference source not found.***)*. The landing acts as an initial joining point for the two bevels, thinner and easier to fuse fully together in a single pass. But due to the thin and short size of the original landing feature, it is eclipsed by the butter passes of nickel and an additional pass is needed to recreate this feature.

Figure 16: Pure Ni Butter Pass Fixturing

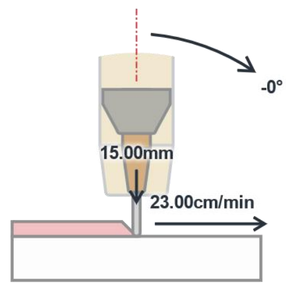

Figure 17: Butter Pass Welding Parameters

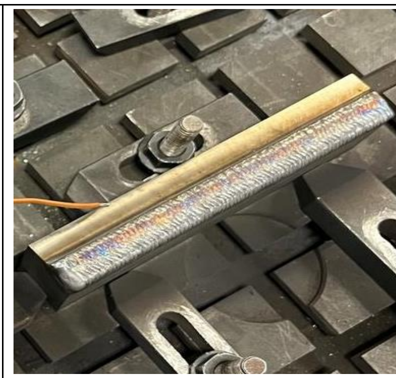

Figure 18: Butter Pass 1, covering first half of U Groove with Pure Ni material

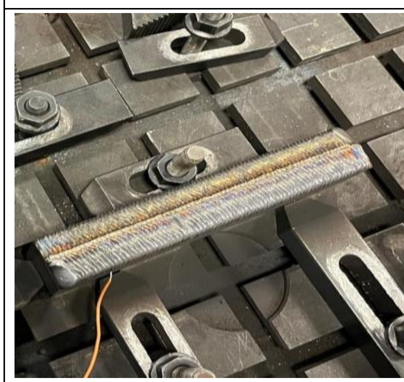

Figure 19: Butter Pass 2, covering second half of U Groove with Pure Ni material

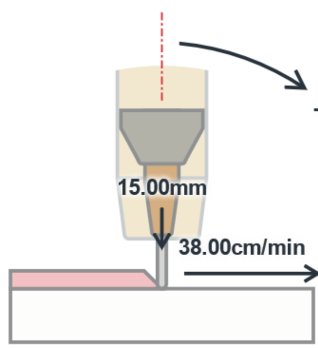

Figure 20: Landing pass welding parameters

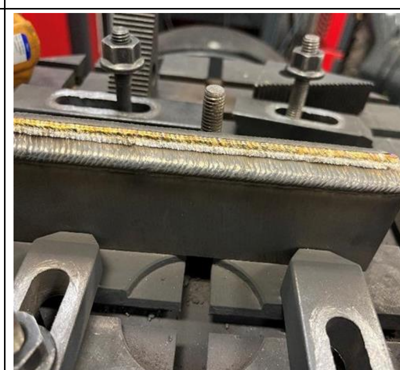

Figure 21: Pure Ni landing pass

Once the landing is recreated with the cast iron contacting material, the second material is now used to join the two sides of the weldment coupon and fill in the remaining weld volume. The first pass of the non-contacting material – in this cast, mild steel – is a root pass, which will fuse the two sides of the weldment coupon along the landing (Figure 22). Depending on the material and geometry of the bevels and landing, a single root pass may be sufficient, or a second one is employed to fully fuse and join the pieces. The welder may need to grind the underside of the first root pass prior to the second root pass to avoid lack of fusion pores or other voids(Figure 23 - *Figure 24*). After the root passes are complete, the remaining bevel volume will be filled by balance welding the upper and lower bevels with the non-contacting material, with a capping pass or passes on each side of the bevel to ensure the volume is entirely filled (Figure 25 - *Figure 27*).

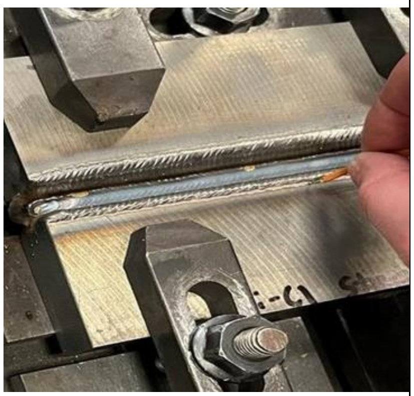

Figure 22: 1st mild steel root pass on upper bevel

Figure 23: Underside of 1st mild steel root pass after grinding

Figure 24: 2nd mild steel root pass on lower bevel

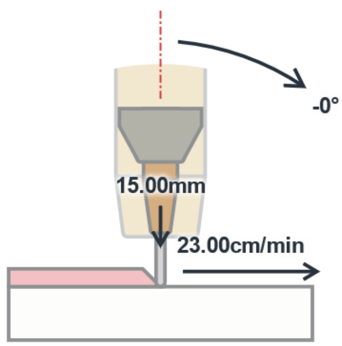

Figure 25: mild steel fill and cap passes welding parameters

Figure 26: Weldment after all mild steel fill passes

Figure 27: Weldment after mild steel cap passes

Consistent with the prior weld categories and shown in the figures, as the type of weld pass – root versus fill versus cap – change, the welding parameters change as well. These changes are often adjusting the travel speed of the weld and wire feed rate to achieve the desired pooling of the filler material.

The weld trials for this category were only partially successful – while the Double U Groove welds using Pure Nickel / Mild Steel were successful, weld attempts with other nickel-based filler materials and mild steel showed promise but were not successful. The observed cracking occurred in the mild steel infill passes along the longitudinal plane, rather than in the butter passes or cast iron itself. Residual stresses in the multi-material weld are expected to be reason for these cracks as no significant metallurgical issues are expected.

Thermomechanical modeling will be pursued to better understand and validate the root cause of the cracking seen and to avoid this issue in the future as larger geometries are explored, but further samples will focus on the successful Pure Ni / Mild Steel combination. While potential other secondary filler materials could be attempted and explored, mild steel is the most promising option for commonly available, low-cost welding metal and is still the best fit for the secondary material used in this program going forward.

Double Material, Double V Bevel:

This weld category saw no successful trials, and the potential source of those failures – in this case, cracking – is both the bevel geometry, as discussed in the Single Material Double V Groove section, and the material combinations, as discussed in the Double Material Double U Groove section. Thermomechanical modeling will be employed to analyze these welds to understand to what degree the bevel geometry, the welding parameters, and the welding materials contribute to the failure modes observed.

Of the 12 MIG weld candidates trialed, 7 were successful – no visible defects or cracking observed – and further iterated for final optimized welding parameters. The key parameters for each pass within each weld have been determined and stored for replication in future welds.

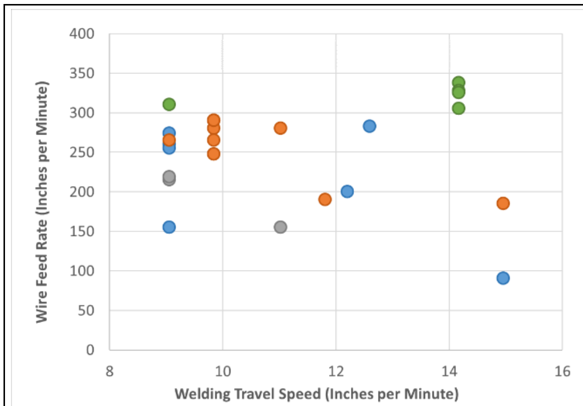

Figure 28: Wire Feed Rate (IPM) vs Weld Travel Speed (IPM)

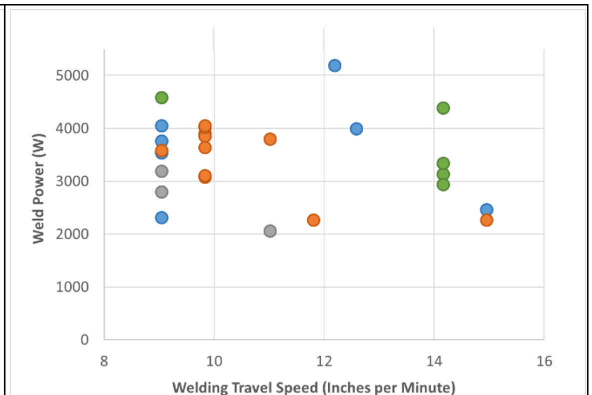

Figure 29: Weld Power (W) vs Weld Travel Speed (IPM)

A selection of those parameters is shown in Figure 28 and Figure 29. The parameters of these welds will be used to replicate these candidate welds in thermomechanical model simulations. Once the model has been validated against measurements and characterization of the physical welds, and adjusted or iterated as needed, the models can be used to better understand and predict the success of future welds. This will allow for the simulation of additional materials, bevel geometries, and updated parameters in a more efficient manner than iterative welding and analysis.

Characterization and testing

Microstructure Analysis:

An essential goal of the welds created in this program is to minimize the thermal impacts of the welding process on the cast iron, specifically the heat affected zone. To validate if the current weld parameters do so successfully, the welds were optically assessed to determine the type and degree of microstructure changes, focusing on the PMZ and HAZ specifically.

As shown in the above images, the material matrix undergoes several changes as you look from the weld center outwards towards the base material – the Area 1 is the filler material itself, in this case a Nickel-Chrome alloy. Where it meets the cast iron base material is the weld boundary,

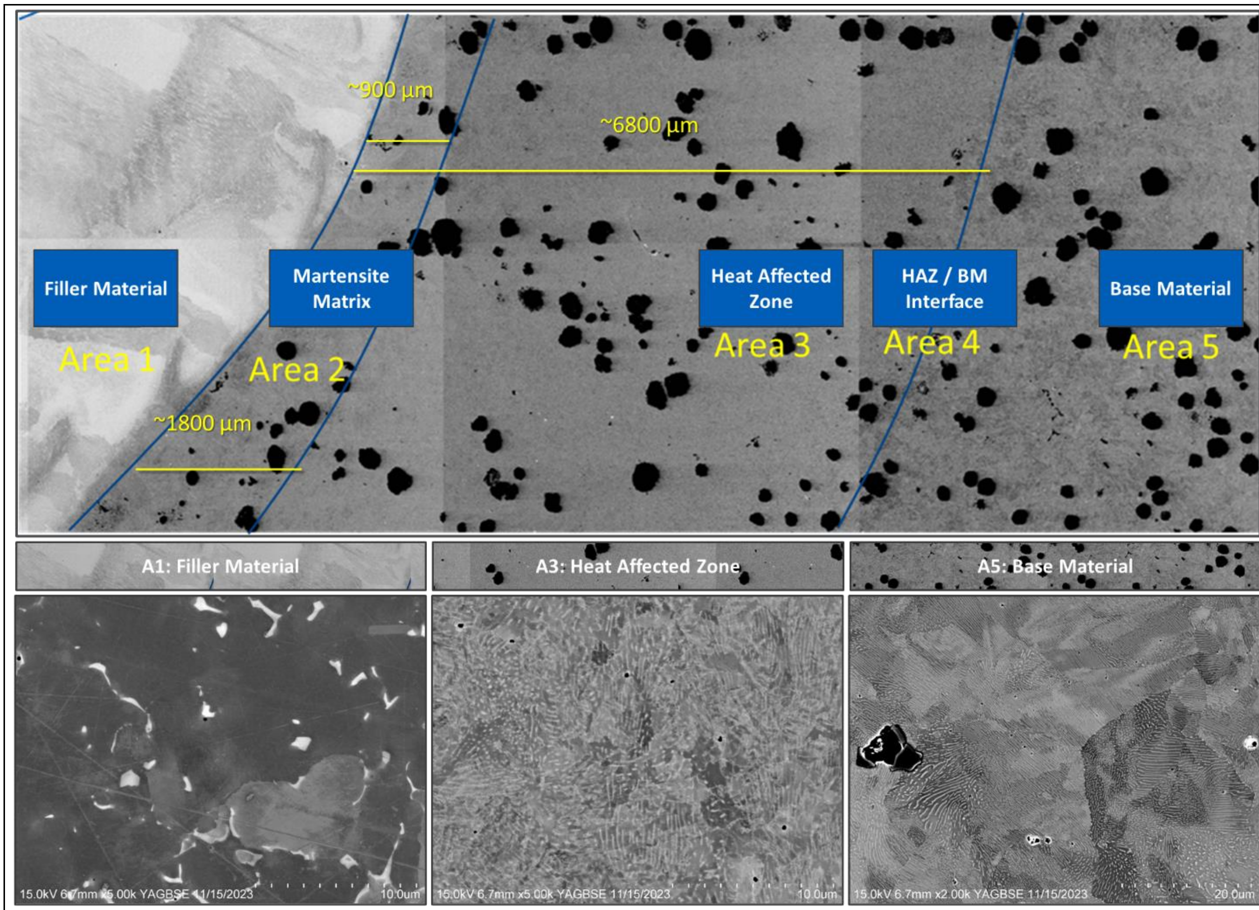

Figure 30: EDS imaging of Nickel-Chrome alloy weld noting the location and size of key material matrixes

leading into the PMZ within Area 2, cast iron is in the martensitic state due transformation by the heat of the weld. In this sample, the martensitic region had a maximum width of 1800 micrometers, or 1.8 mm. A properly optimized welding process and parameters should ensure this region is minimized, as the brittle nature of the martensitic phase is sensitive to cracking in the base material. Area 3 is the wider HAZ, where the cast iron material is still impacted by the thermal impacts of the weld but does not lead to martensitic transformation – the material in this region is a spheroidized cementite. Area 4 marks the transition from heat-affected cast iron to the base material itself, with Area 5 being unaffected base material ductile cast iron.

Defect Detection and Analysis:

Optical imaging is very useful when evaluating the quality of welds, specifically to confirm the presence and type of defects found within welded samples. Some defects may be immediately visible, such as surface cracking between weld beads or along the base material. But many defects are internal to the weld and only visible after sectioning, polishing, and imaging. Even when a defect is immediately visible, the full scale and shape may not be visible without further sectioning. For example – while the crack between the cast iron base material and Nickel-Chrome alloy welding material shown in Figure 31 would have been visible without imaging, the length and path of the crack as it moves along the PMZ and into the root pass would not have been clear without imaging.

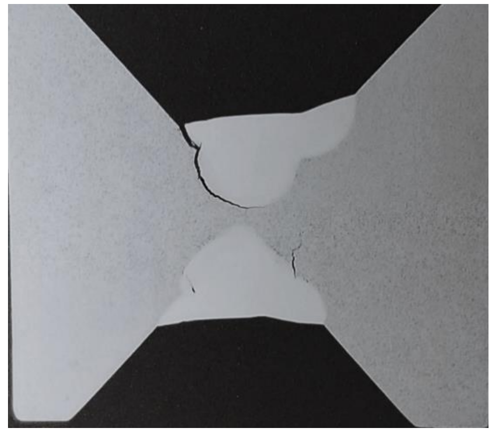

Figure 31: Image of cross section cut from cracked LHW welded V bevel sample

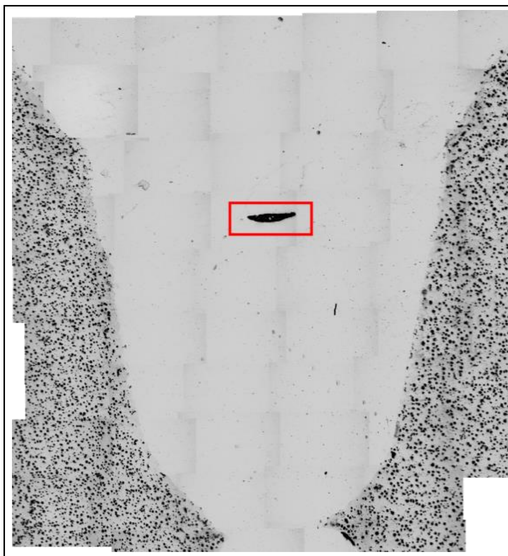

Figure 32: Lack of fusion void within the Nickel-Iron alloy region of weld

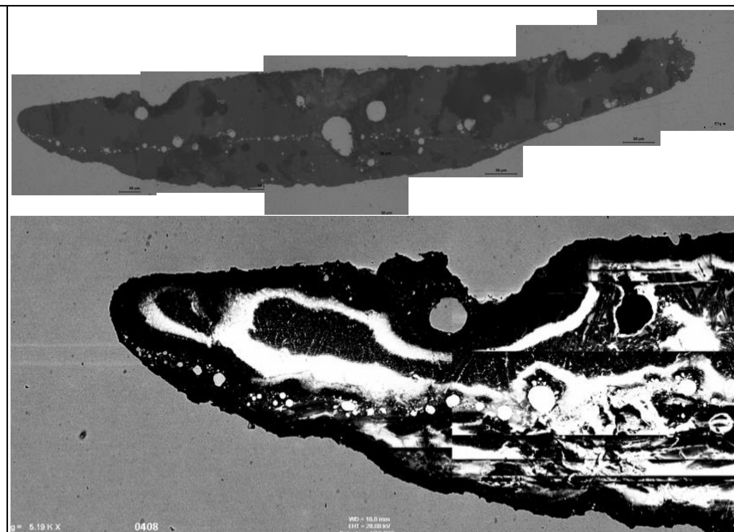

Figure 33: Magnified images of lack of fusion void

Other defects, like the pores shown in *Figure 32 - Figure 37* are fully internal to the weld were captured through sectioning and polishing. The most common defect found in the optimized welded samples was porosity, lack of fusion pores specifically. This indicates that some further parameter optimization of the root pass parameters may be required to ensure full fusion of the weld beads to the root face and bevel walls. Parameter updates could include lower welding speed, increased wire feed rate, slightly increased weld power and a dwell on the bevel faces.

Figure 34: Potential lack of fusion pore at root face bevel wall

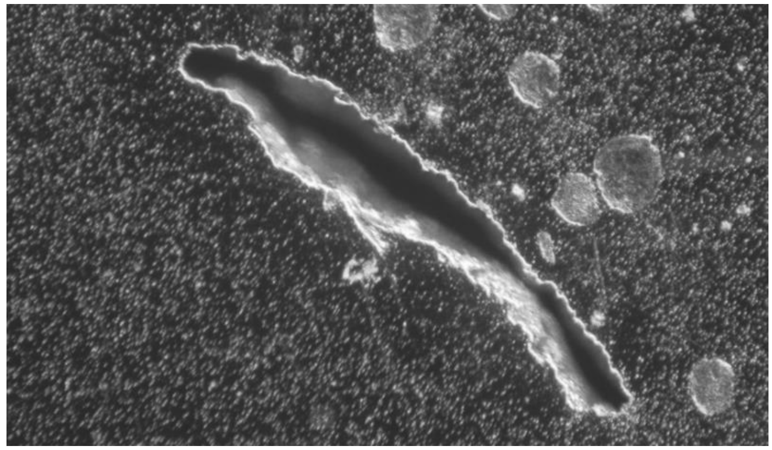

Figure 35: Void with metallic inner surface - spherical gray inclusions in upper right are graphite nodules in cast iron HAZ

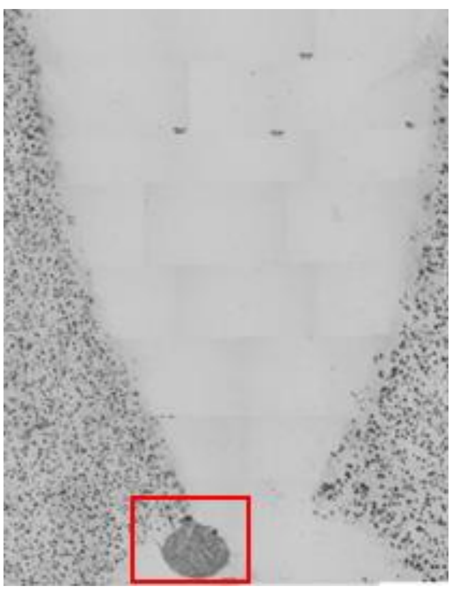

Figure 36: Pore and interstitial feature in Pure Ni U Bevel weld

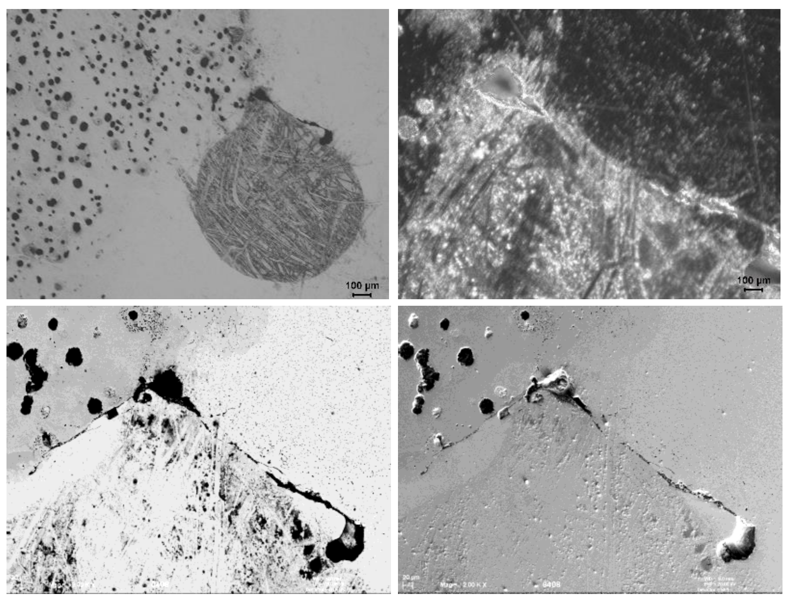

Figure 37: Various contrasted optical images of pore at root face of bevel, potentially due to lack of fusion on root pass.

In the case of the LHW welded samples, the more common issue was cracking. Cracking was specifically seen at or near the heat affected zone, propagating through the graphite nodules in the heat-affected cast iron base material. In *Figure 38* the defect is a toe or underbead crack which almost fully separated the welding material deposited from the heat-affected cast iron, likely due to martensite-embrittlement and/or hydrogen assisted cracking. The crack characteristics observed in *Figure 39* and *Figure 40* are associated with cold cracking due to embrittlement via martensite formation and/or hydrogen assisted. This cracking is expected to have occurred after the base materials cools below approximately 200 C.

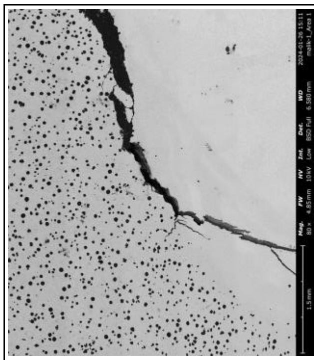

Figure 38: Crack along weld boundary in nickel alloy LHW V Bevel

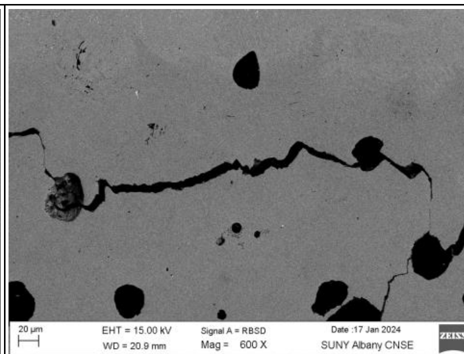

Figure 39: Crack propagating between graphite nodules in Nickel-Chrome alloy LHW welded V Bevel

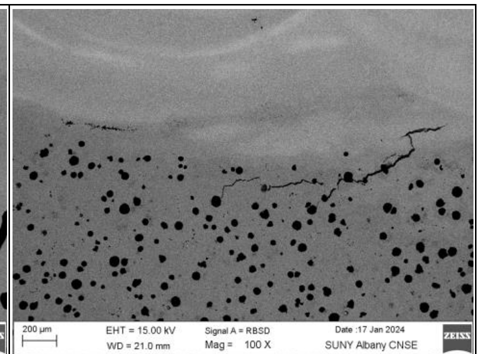

Figure 40: Crack propagating into weld material and base material in Nickel-Chrome alloy LHW welded V Bevel

EDS Analysis:

SEM / EDS imaging was used to obtained high magnification imaging and compositional information.. This is particularly useful in the case of multi-material welds, where the presence, quantity, and location of discrete elements can be used to gauge the level of melting, fusion, and defects of the materials in the weld section.

An example of this analysis is shown in Figure 41, a line scan taken across the base material, HAZ, and into the welded region of a MIG-welded U Groove sample, welded with Pure Nickel filler. The orange line denotes the presence of iron (Fe) at each point along the line scan. Nickel (Ni) is the primary element present in the weld filler materials and is shown with a blue line. The Fe line is high throughout the base material section (0 - ~120 µm). In the HAZ region (~120 - ~160 µm) the Fe plot declines, and the Ni line increases as the two materials blend within the partially melted zone. Once within the weld fill region (~160 µm onwards), the Ni content is relatively stable and Fe at a steady lower value. The remaining elements in the chart are consistent at low values across the scan, excepting a few spikes where the line crosses the spherical shapes scattered throughout.

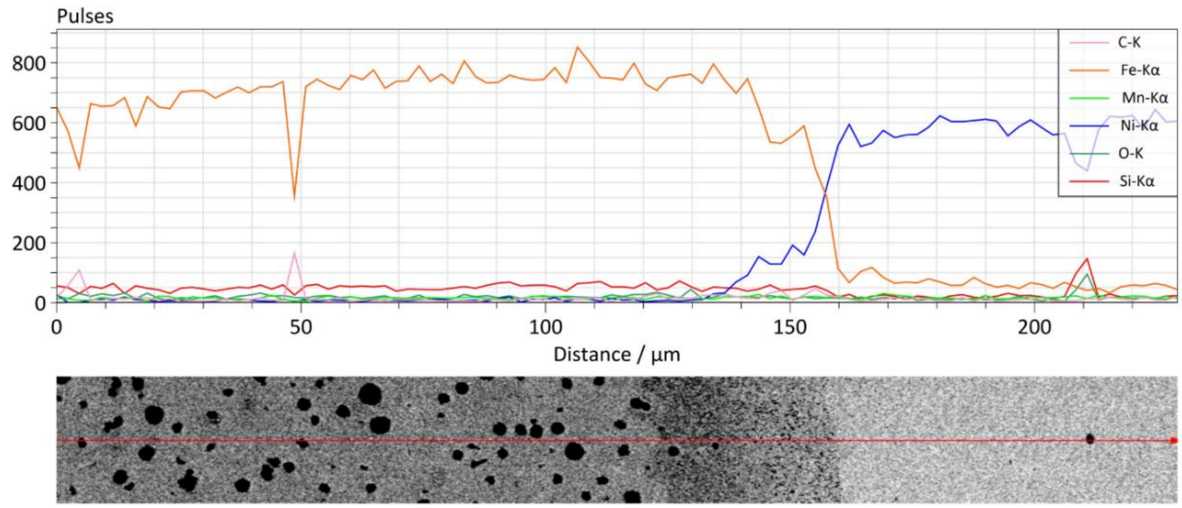

Figure 41: Line scan of Pure Ni weld showing presence of key elements across the cast iron, HAZ, and into weld filler material

In the following images, you can see similar spherical and irregularly shaped spots on the optical image of a Pure Ni MIG-welded sample, along with darker lines running along the weld boundary, indicated by the change in color and pattern from the upper left to the bottom right regions. At first glance, it can be difficult to assess which of these dark spots are pores, voids, etc. With element analysis, it becomes clear that the spots in the upper left (cast iron) region are graphite nodules, visible in pink in Figure 43, whereas the two larger spots along the weld boundary are lack-of-fusion voids, as they are black in the element-coded image as well. These voids and the cracks emanating from them are a defect that indicates an iteration in welding parameters is needed to ensure proper fusion of the weld bead and base material is achieved both at the weld root and along the bevel walls. In contrast, images taken from a section of the PMZ of a Nickel-Iron alloy weld are shown in Figure 44, showing the same segment with and without element analysis. In this area of the weld element analysis can confirm that the spherical inclusions are graphite nodules and not voids or defects which need to be addressed.

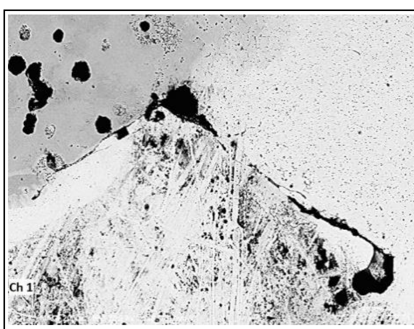

Figure 42: Lack of fusion void in Ni weld leading to cracking along weld interface

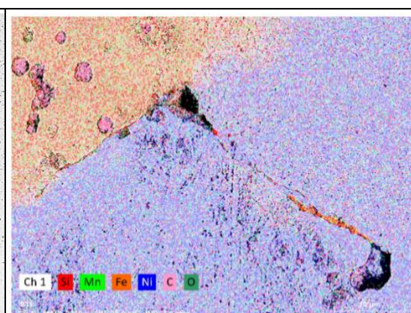

Figure 43: EDS scan of lack of fusion void in Ni weld, individual elements shown by color

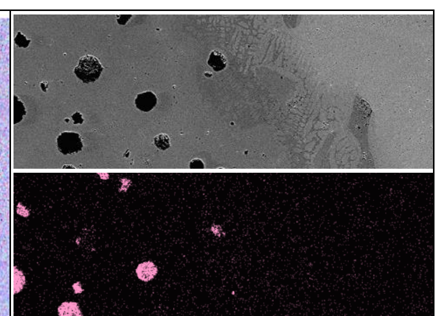

Figure 44: EDS imaging of Nickel-Iron alloy weld PMZ, without and with carbon element analysis

Hardness Testing:

Along with the optical characterization efforts to characterize and understand the variety of materials, microstructures, and potential defects across the weld profile, testing was conducted to assess the material properties and performance of welded samples. Further mechanical testing is planned for this program, but the efforts described in this document are early-stage tests conducted to review material properties across the various candidate welds to aid in downselection. Future testing will aim to standardize mechanical performance across multiple samples from the downselected and optimized weld(s) and compare it to directly to the baseline material properties.

The first test conducted for characterization was Hardness Testing – measuring the force required to indent into a material over a small area, resulting in a Vickers Hardness Number (HV) that corresponds to the kilograms of force required to create a 1 mm² indent. This test was a useful one during characterization and downselection as it can be conducted in a line across the weld profile; changes in the HV value across the profile can indicate shifts in both microstructure and material.

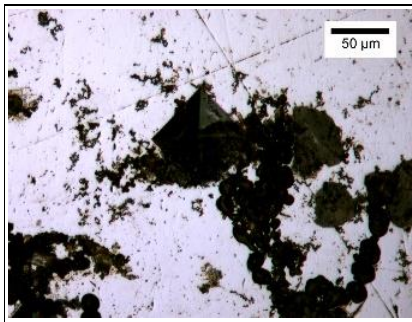

Figure 45: Hardness indents in cast iron region, through graphite nodules - 130 HV

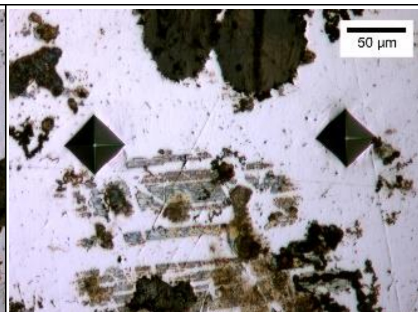

Figure 46: Hardness indents in cast iron region, avoiding graphite nodules - 350 HV

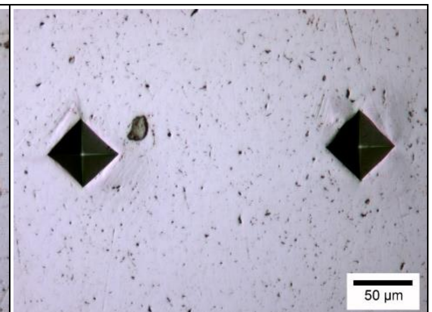

Figure 47: Hardness indents through Nickel-Chrome alloy weld fill region - 270 HV

In Figure 45 - Figure 47, the Vickers value changes as the indents target different materials across the profile. In Figure 45, the indent is placed in a darker area of the base material HAZ, in what we confirmed through optical analysis to be a graphite phase. In Figure 46, the indent is made nearby in the same general region but avoiding any dark areas of carbon (graphite nodules), leading to significant higher HV value, as the cast iron is a harder material than graphite. Figure 47 shows an indent through the weld fill region, where the Nickel-Chrome alloy has a hardness value somewhere midway between the two base material region values. Vickers readings can be used to estimate or confirm the materials present in a given region and are particularly useful to indicate the location of the HAZ.

See Figure 48, where an annotated hardness plot shows the hardness values, indent images, and material region of each point across the weld profile. While the base material region has a fair amount of variance – namely, sharp valleys where the indents hit a soft area of graphite – the upper range of this region is fairly consistent. As the indents approach the bevel area of the weld the values will grow higher on the exterior of the well region – the cast iron HAZ has undergone microstructure changes due to the heat input during welding and is embrittled. Once into the weld fill region, the values are very consistent across the profile until the indents once again near the HAZ and begin to rise.

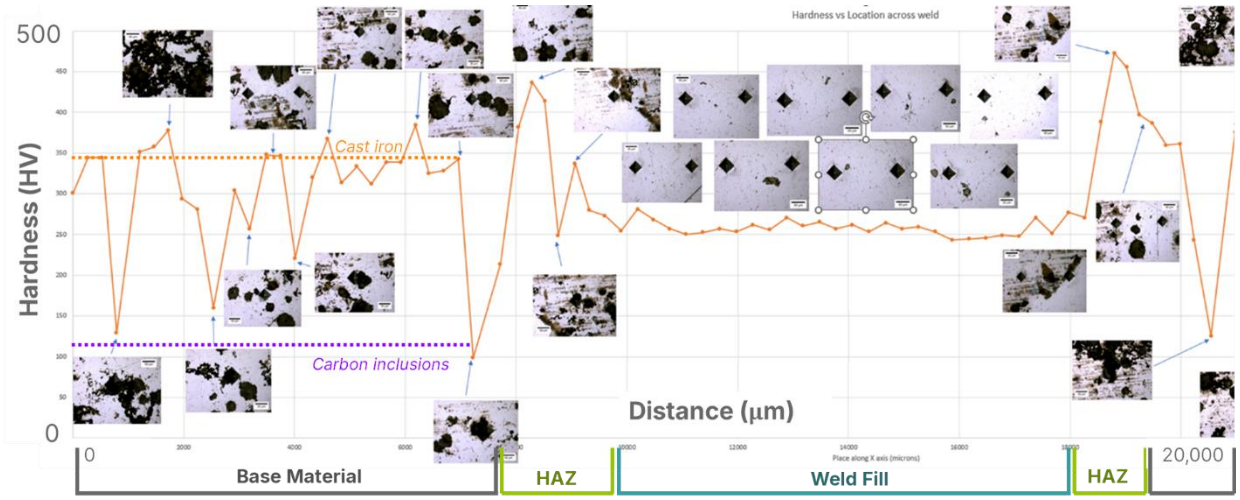

Figure 48: Hardness values across weld profile, annotated with indent images and notes on weld regions

Hardness plots can verify material and microstructure changes across the weld profile, providing a visual representation of the weld regions and in some cases a method of comparison between welds of the same material. The high points of hardness across the weld profile indicate the location of the weld interface and can be used to compare the size and impact of the HAZ between two welds of the same material but different parameters, making it a useful and efficient testing method during downselection.

Mini-Tensile Testing:

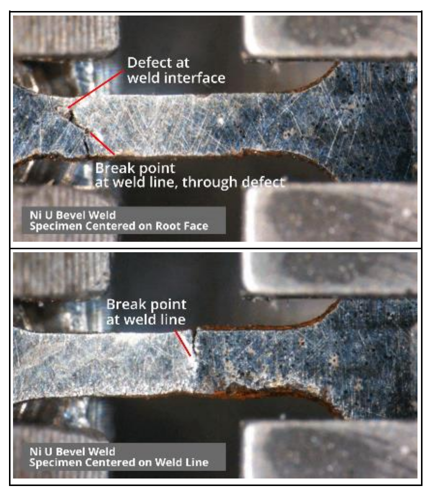

While tensile testing of any kind, even mini-tensile testing, is more involved in sample preparation and post processing than hardness testing, this test was a valuable mechanism to characterize the welded samples strength and failure modes under tension. Samples from seven optimized MIG welds were used to create several mini-tensile specimens per weld and tested to assess the failure location – through a defect, in the cast iron, in the weld material, or at the weld boundary – and the strength of the weld in that location. Figure 49 shows images from four of those tensile tests, moments before the samples failed. Even in cases where there was a defect present in the weld fill or cast iron regions, the specimens consistently failed along the weld boundary, as expected. To determine how consistent this failure mode remained, the specimens were cut to center the gauge length either along the weld boundary itself, or with the root face and weld filler region centered. Due to the difference in strength between the cast iron and the Ni-based weld fillers, the variation in center point changes the effective strength of the materials in the gauge strength. However, both the on-center and off-center samples consistently failed at the weld line, regardless of the percentage of cast iron versus filler material in the gauge section.

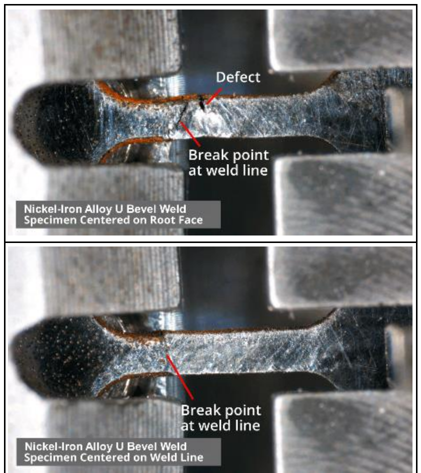

Figure 49: Break points of mini tensile specimens centered along root face or weld line

This data was useful for preparing for future tensile testing with full size specimens, as well as qualitatively assessing the presence and impact of welding defects during failure. Completed mini-tensile testing data is shown for two materials, a Nickel-Iron alloy, and Pure Nickel, in Figure 50 and Figure 51, respectively. Prior tensile testing of a Nickel-Chrome alloy deposited on cast iron is included below in *Figure 52*, with an approximately 80,000 PSI UTS, or around 550 MPa, in a similar range to the completed mini-tensile data.

The mini tensile testing will be followed by full-scale tensile and fatigue testing using optimized specimens from the shortlisted welds samples – 6 single material MIG welds and 1 double material MIG weld. This additional testing will further validate candidate weld downselection, along with the initial testing data used for indication of weld failure modes and tensile strength and will be compared to full-scale tensile and fatigue data for baseline cast iron to establish what degree of strength debit is created by the welding process.

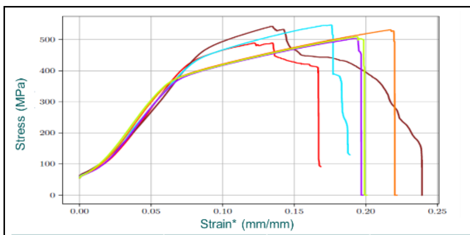

Sample Name	UTS (MPa)	0.2% YS (MPa)	Break Strain* (mm/mm)
Ni Fe Alloy_Centered_1	489.09	444.19	0.168
Ni Fe Alloy_Centered_2	542.33	493.71	0.239
Ni Fe Alloy_Centered_3	546.80	423.22	0.189
Ni Fe Alloy_Off Center_1	504.03	369.65	0.198
Ni Fe Alloy_Off Center_2	531.58	363.61	0.222
Ni Fe Alloy_Off Center_3	509.21	359.49	0.201

** Break Strain values calculated through cross-head displacement*

Figure 50: Plot and data for mini-tensile testing of Nickel-Iron alloy welded to cast iron

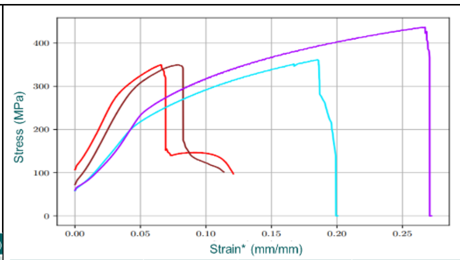

Sample Name	UTS (MPa)	0.2% YS (MPa)	Break Strain* (mm/mm)
Pure Ni_Centered_1	349.68	317.62	0.121
Pure Ni_Centered_2	349.80	313.26	0.114
Pure Ni_OffCenter_1	361.48	219.76	0.201
Pure Ni_OffCenter_2	436.70	256.87	0.272

** Break Strain values calculated through cross-head displacement*

Figure 51: Plot and data for mini-tensile testing of pure Nickel welded to cast iron

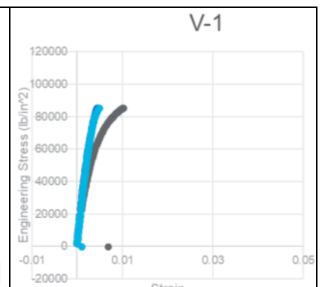

Figure 52: Strength testing of Nickel-Chrome alloy deposited on cast iron, early feasibility work

Downselection of Final Welding Evaluation

Welding Process Optimization:

Welding process optimization resulted in seven out of twelve attempted MIG (Metal Inert Gas) welds successfully created with no failure-causing defects at 1” heights. Six of these welds are single-material, consisting of a nickel-based welding material used to join ductile cast iron bevels. Three welding materials were used on two bevel designs, a Double U Groove, and a Double V Bevel, all using balance welding. The seventh successful weld was a multi-material weld consisting of pure nickel coating ductile cast iron Double U Groove bevels and joined together with mild steel. The five unsuccessful welds were other multi-material welds with varying material and bevel configurations. The seven successful MIG welds remain candidates for downselection.

LBW / LHW welding process optimization has been thus far unsuccessful to create a defect – free weld over 0.25” in height. Further experimentation with process parameters and equipment optimization, combined with thermomechanical modeling could lead to further successful trials but LBW welding was overall found to be a less-successful option and not a contender for present downselection. See Deliverable 2.1 Welding Process Optimization Summary for a full review of these processes and key learnings.

Characterization of Welded Samples:

The characterization of welded samples used weld samples and specimens created during or immediately after the optimization process to analyze and assess the characteristics and quality of welds created. The characterization data was particularly useful during the optimization process to better understand and detect potential defects in the weld which could be avoided with further parameter iterations. See Deliverable 2.2 Characterization of Optimized Welded Samples for a full review of the characterization processes and learnings.

Characterization data was also used to validate the quality of the seven successfully optimized welds, verifying that there were no failure-causing defects created by the processes and that the welds had sufficient strength to meet the 40% debit criteria set for the second Go / No-Go decision. The 7 successful candidate MIG welds show consistent and acceptable results for the following downselection criteria:

- Heat Affected Zone (HAZ) Size: The HAZ for each weld was consistent and achieved the goal for a minimized, determined from both optical and testing processes
- Defect Presence: The welds were crack-free and had no other failure-causing defects observed during optical analysis
- Weld Performance: The welds had sufficient fusion and integrity to join the welding material with the base material and when loaded under tension, the welds failed at the weld line or within the weaker weld fill material, rather than in the stronger base material. Initial tensile testing data showed the weld strength to be above the 40% debit threshold set.

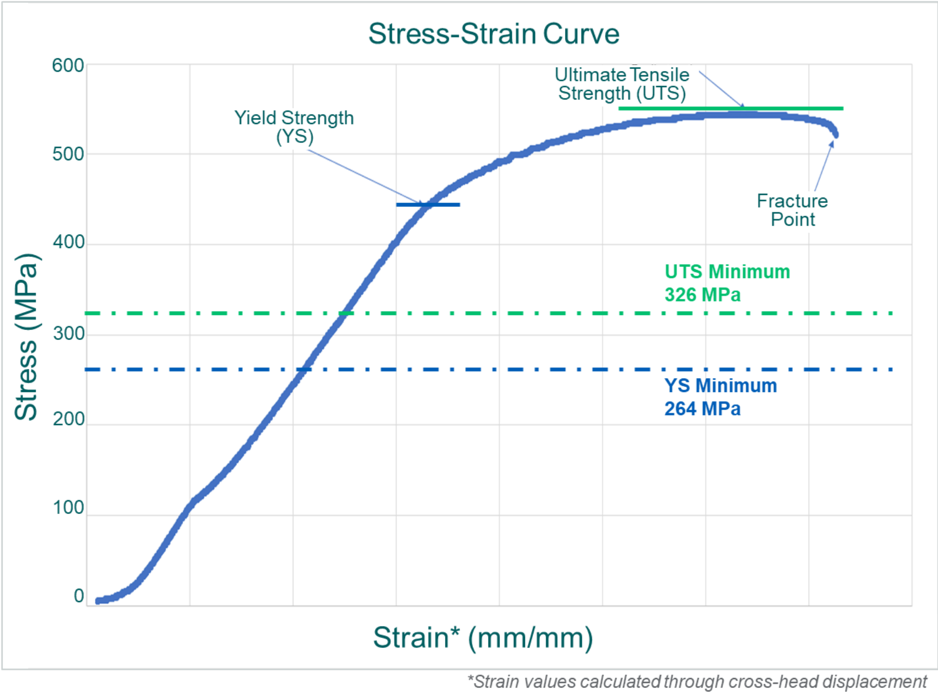

Figure 53: Tensile testing data of baseline cast iron, noting the yield strength and ultimate tensile strength and their 40% debit thresholds in blue and green, respectively

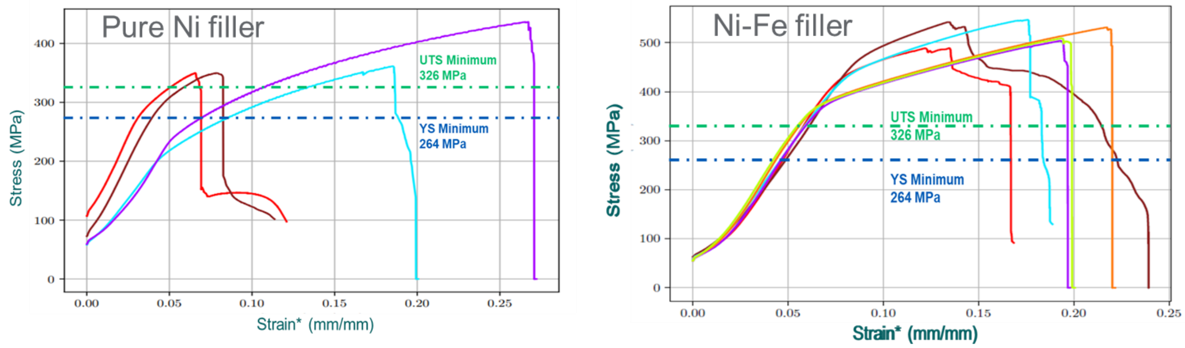

Figure 54: Mini-tensile testing data for Pure Nickel and Nickel-Iron alloy welded samples, showing Yield Strength (YS) above the 40% debit threshold (blue line) and Ultimate Tensile Strength (UTS) above the 40% debit threshold (green line)

Welding Material	**UTS (MPa)**	**> 326.03 MPa UTS Threshold**	**0.2% YS (MPa)**	**> 263.97 MPa YS Threshold**
Pure Nickel *Sample Average*	520.51	Yes	408.98	Yes
Nickel-Iron Alloy *Sample Average*	374.42	Yes	276.88	Yes
Nickel-Chrome Alloy *From Feasibility Work, Average*	551.58	Yes		

Weld Cost:

The other criteria set for the second Go / No-Go was that of an estimated 8-12% total cost savings for a welded cast iron component cast in subsections and assembled via welding in the USA, compared to the current methods of offshore casting and bolted assembly. Using the cost model developed in D1.3, updated as needed for the specific welding processes, parameters, and material costs, the viable candidate welds were assessed over a variety of scenarios. The most cost-effective mechanism is the multi-material weld, as the usage of relatively high-cost Nickel-based welding materials is minimized by using a secondary, far less expensive welding material: Mild Steel.

Step	International, Bolted Assembly (Current Method)	US Based, Welded Assembly (Proposed Method)	Delta*
Casting of Subcomponents	53.1%	85.6%	+ 32.3%
Shipping (International)	29.0%	0.00%	- 29.0%
International Taxes / Tariffs	13.3%	0.00%	- 13.3%
Shipping (Landed)	2.8%	2.8%	0.0%
Assembly (Machine + Labor)	0.6%	0.7% - 0.8%	+ 0.1%
Assembly (Materials)	0.8%	0.4% - 0.9%	- 0.2%
Post-assembly Inspection	0.3%	0.4% - 0.5%	+ 0.2%
Total:	100%	89.9% – 90.5%	- 10.0%

** Delta given for a 3-welding machine, 24% contacting material usage rate scenario of welding model. Range in prior column covers 3 welding scenarios*

Figure 55: Cost modeling assessment for multi-material welds ranging from 17% - 34% contacting materials, showing saving are within 8% savings threshold

However, even when the weld volume consists entirely of the Nickel-based materials, the savings created are still within the 8% Total Cost Reduction criteria, so long as the weld is a U-Groove design. Due to the wider angle of the V-Bevel, at the approximately 4” height of the final weld design, the volume of welding material needed is far greater in the V Bevel designs compared to the U-Groove. While the Pure Nickel / Mild Steel MIG weld is the best performing within the weld cost metric, the 3 successful Single Material U-Groove welds are still within the success criteria as well.

Final Downselection:

The final downselection process considered the criteria and data summarized in the subsections above – the success of process optimization, the quality and strength of the optimized welds, and the relative cost of the weld process and weld design. Based on these criteria, the initial 24 candidate welds (12 MIG, 12 LHW) were narrowed down to four successful, downselected welds. All four welds are created using an optimized MIG welding process. Three of these four welds are single-material, and all Double U-Groove designs with three different welding materials: Pure Nickel, a Nickel-Iron Alloy, and a Nickel-Chrome alloy. The final selected weld is a multi-material Double U-Groove weld, consisting of Pure Nickel and Mild Steel. See the table below for a breakdown of each candidate weld and its relative success (indicated by color) across the downselection criteria.

Candidate Welds							
Weld Fill Material		Bevel Type	Weld Process	Optimized Process?	Welding Defects?	Sufficient Weld Strength?	Weld Material Cost
Single	**Nickel**	**U**	**MIG / ~~LHW~~**	Yes	No	Yes	$$
	Nickel	V	MIG / ~~LHW~~	Yes	No		$$$
	Nickel-Iron Alloy	**U**	**MIG / ~~LHW~~**	Yes	No		$$
	Nickel-Iron Alloy	V	MIG / ~~LHW~~	Yes	No		$$$
	Nickel-Chrome Alloy	**U**	**MIG / ~~LHW~~**	Yes	No		$$
	Nickel-Chrome Alloy	V	MIG / ~~LHW~~	Yes	No		$$$
Double	**Nickel / Mild Steel**	**U**	**MIG / ~~LHW~~**	Yes	No	*Testing in progress*	$
	Nickel / Mild Steel	V	MIG / ~~LHW~~	No	Yes	*No testing planned*	$
	Nickel-Iron Alloy / Mild Steel	U	MIG / ~~LHW~~	No	Yes		$
	Nickel-Iron Alloy / Mild Steel	V	MIG / ~~LHW~~	No	Yes		$
	Nickel-Chrome Alloy / Mild Steel	U	MIG / ~~LHW~~	No	Yes		$
	Nickel-Chrome Alloy / Mild Steel	V	MIG / ~~LHW~~	No	Yes		$

Bolded welds are the final downselected processes / weld designs
Processes with a strikethrough indicate that no successful welds were created at 1" height thus far

Figure 56: Downselection summary table noting success of candidate welds across several criteria

Full Scale Mechanical Testing

Design for Fatigue and Tensile Testing.

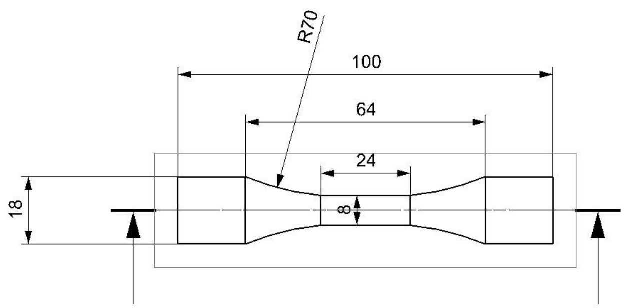

Figure 57: Tensile and Fatigue test specimen design

The design in Figure 57 was made by following the criteria recommended by ASTM and meets all the requirements of ASTM E466 for testing fatigue. For the sake of uniformity, the same design was used for both fatigue and tensile testing.

Heat treatment

The samples were heat treated for 8 hours at 200 °C followed by air cooling to room temperature. Welding produces significant stresses on the samples and this stress relief procedure, that was empirically derived from GE's past work, was utilized for this study.

Specimen manufacture

Our experimentation involved 7 different welded samples of different deposited materials. They are:

- Ni-Cl U-shape – Batch A
- Ni-Cl V-shape - Batch B
- Inconel 625 U-shape – Batch C
- Inconel 625 V-shape - Batch D
- Ni-Cl steel U- Shape - Batch E
- Ni-Fe-Mn U- Shape - Batch F
- Ni-Fe-Mn V- Shape - Batch G

Upon receiving the samples, they were sectioned, profiled, and polished to produce full size tensile test specimen. The procedure followed involved:

- **Cutting the samples:**
  The welded samples were sectioned using a bandsaw, to make 5-6 rectangular blocks from each welded plate as shown in Figure 58.
- **Turning of bars:**
  Turned these rectangular blocks into circular bars using a manual lathe.
- **Profile making:**
  Made the profile of the dog bone shape specimens using a CNC lathe per ASTM recommendations of roughing and finishing to minimize work hardening.
- **Polishing**:
  Polished the specimen with sandpaper to get rid of any burr and other stress concentration points. For fatigue specimens, targeted a 0.2 micron surface finish, and for tensile samples, targeted a 0.2 to 0.3 microns as recommended by ASTM E466 for fatigue and ASTM E8 for tensile. All the specimen used in this study met these target values.

a) Cutting samples b). Turning into bars c). Profile making d). Polishing

Figure 58: Tensile and fatigue test specimen preparation

Inspection and visual analyses:

After polishing, samples were evaluated for defects. A few of the samples exhibited porosity within the gauge cross sections. Examples with defects were imaged and are shown in this section.

Specimen-A

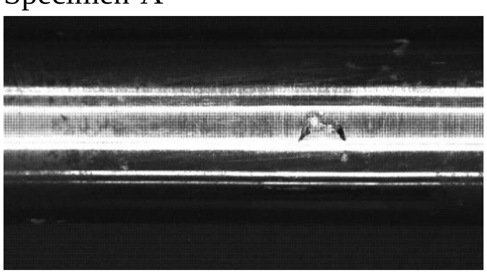

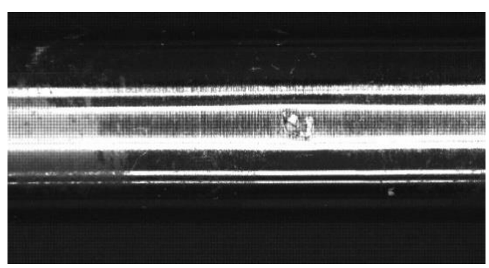

Specimen- B

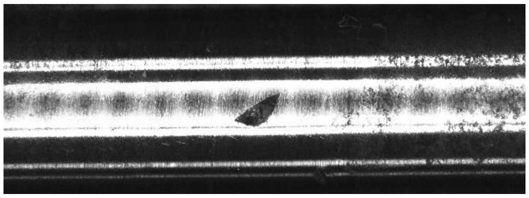

Specimen- C

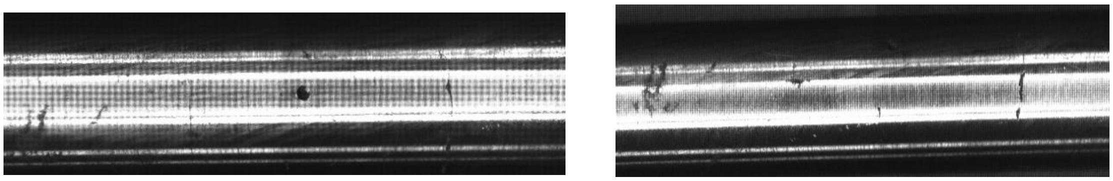

Figure 59: Macro images of defects observed within the gage of the welded tensile samples. Defects primarily appear to process originating defects likely due to insufficient fusion

Specimens testing and results:

Utilizing a universal testing frame from MTS, tensile tests were performed on samples at a strain rate of 10^-3/s. The specimen diameter is 8mm and the gauge length is 24mm. Figure 60 and Figure 61 are a compilation of the test results compared to baseline cast iron.

It can be observed that the baseline cast iron has the highest UTS and among the highest yield of any material under investigation in this study. This was anticipated and confirmed. When repair of cast iron is performed, the nature of the welding process and the dissimilar materials usage will lead to some strength debit in the resulting repaired product. This was observed across the board in the tensile testing data presented in Figure 60 and Figure 61. But too much of this debit will lead to poor end use load applicability and therefore, at the outset of this study, threshold strength debit values were determined and used as targets for selection and shortlisting of welds.

The threshold strength debit values were determined to be 158 MPa in yield and 255 MPa in UTS. As observed in Figure 60, multiple materials in both the U and V groove type welding met these threshold criteria of strength debit. This allowed this research team to shortlist them for further study.

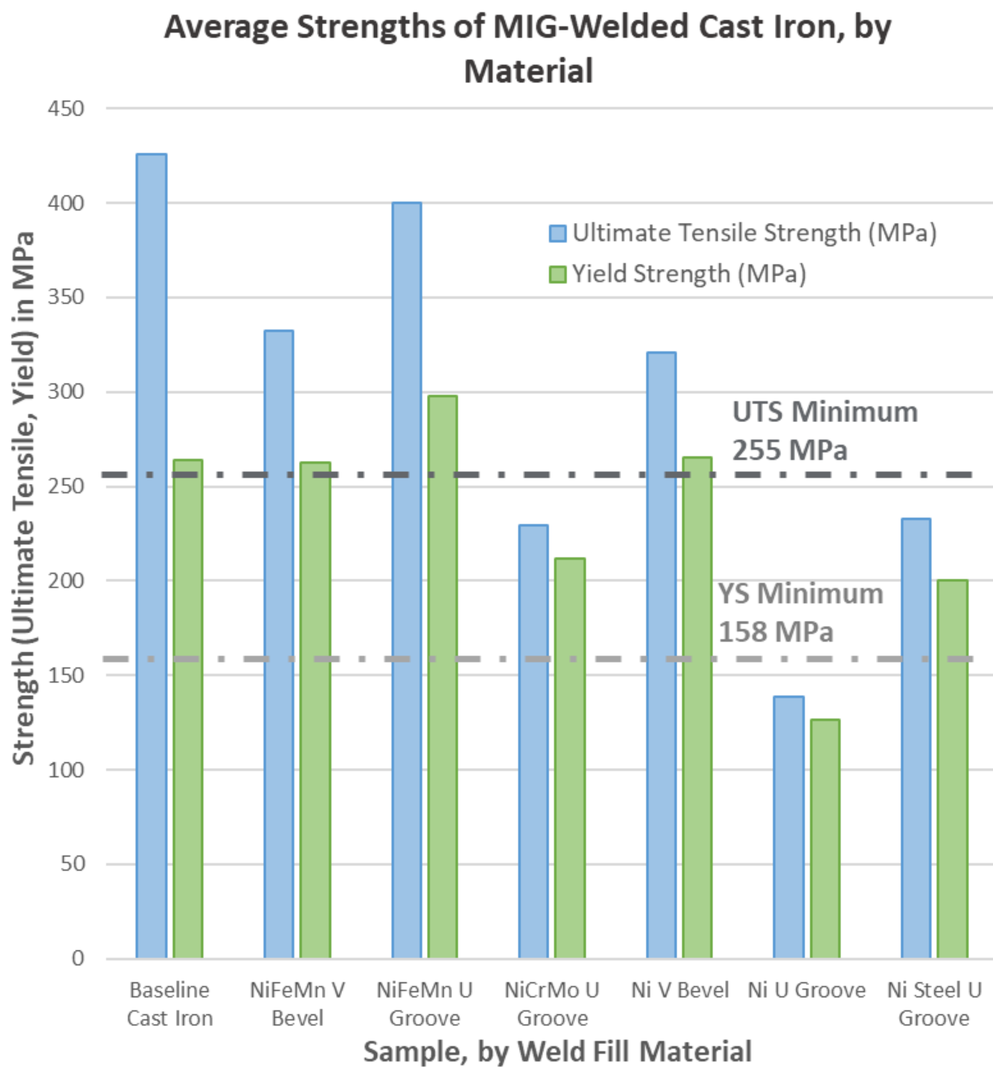

Figure 60: Comparison of the strengths of various weld materials with baseline cast iron data.

While strength debit could be attributed to weld stresses, material transformation from welding and material inhomogeneity effects themselves, during the course of the study, this research team identified significant scatter in the tensile data as shown in Figure 5. This warranted further study of these tensile test samples through the use of fracture surface analyses.

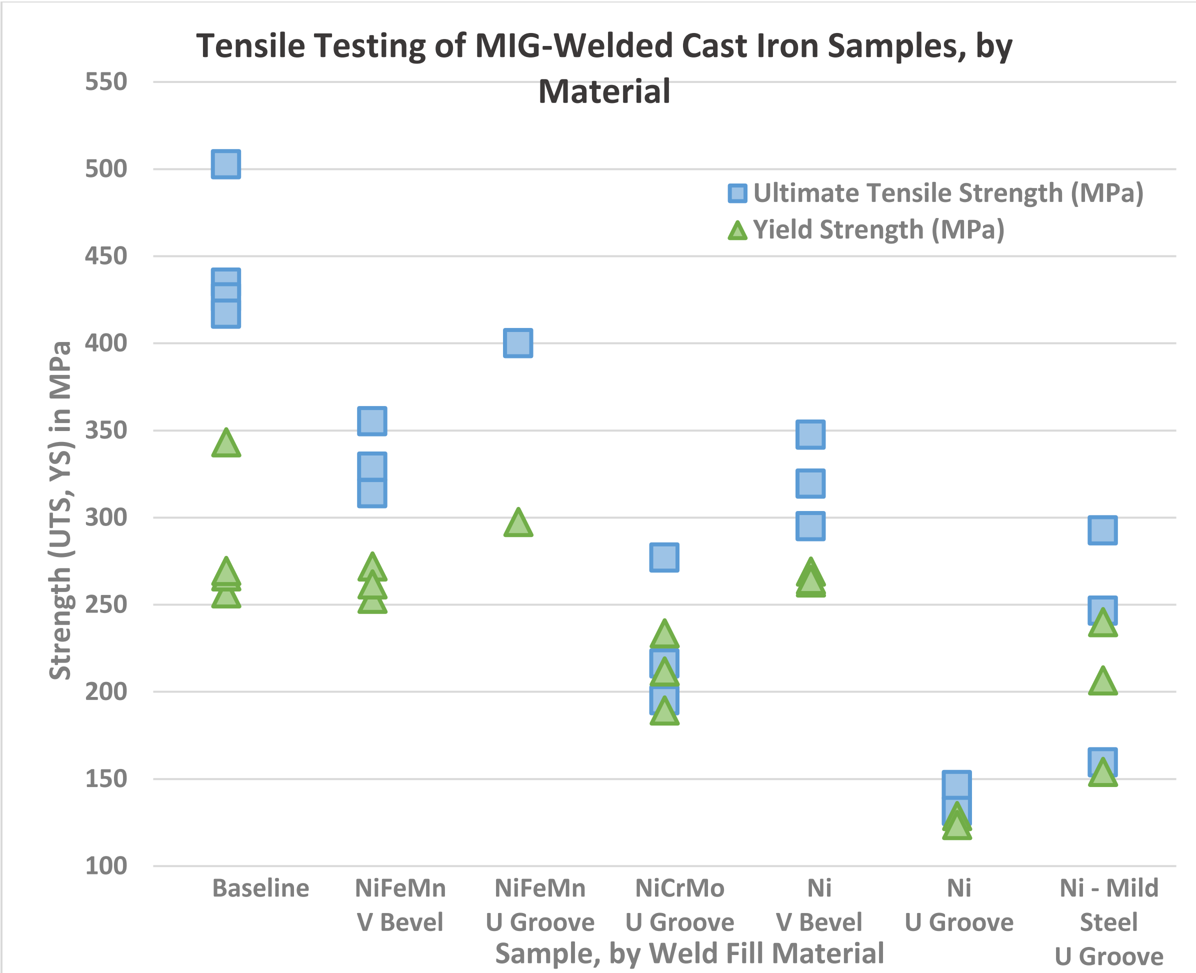

Figure 61: Comparison of the strengths of various weld materials with baseline cast iron data.

A detailed analysis of the fracture surfaces of all the specimen used in tensile testing revealed process defects. Process defects are pores and delamination in the weld material potentially resulting from material inhomogeneity and material transformation around the heat affected zones. The fracture surface analyses also indicated failures mostly at the weld lines and their mechanisms are detailed in the forthcoming sections.

Fracture surface analyses of tensile specimen.

Fracture surface analyses of the tensile specimen indicated that the failures mostly initiated and propagated along the weld line.

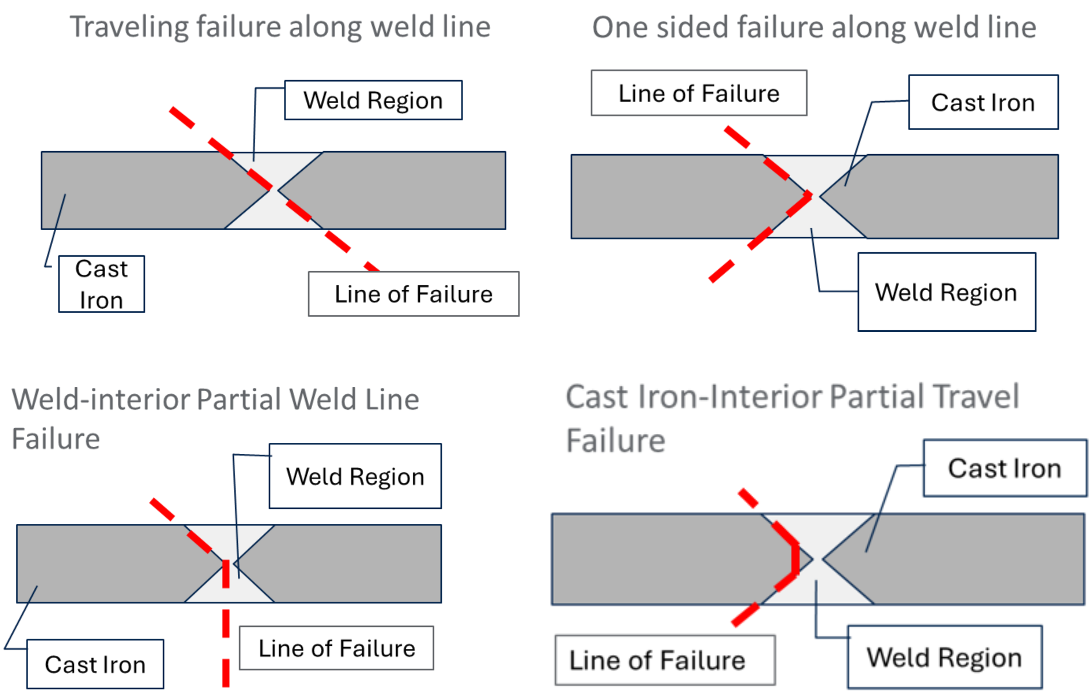

Figure 62: Types of failures observed in the tensile test samples.

The first two types of failures, initiated and propagated entirely along the weld lines. In some cases, the failure started on one side of the weld and jumped or travelled across the root pass due to its poor penetration characteristics achieved during the weld. This root pass penetration, or lack thereof, is a common problem that leads to failure of the weld.

In other cases, the failure initiated and propagated on the same side of the cast iron-weld interface called a one sided failure. In these cases, the root pass penetration was adequately achieved presenting the failure to travel across the weld. But the bond between the two dissimilar materials is still the region of highest stress concentration, and where the failure occurred. This was confirmed through simulations models developed through this study to replicate this weld behavior.

When root pass penetration and adequate metallurgical bonding were achieved, occasionally, the failure initiated along the weld line, but propagated into the weld material. Based on tensile results presented, the weld material has lower strength and higher elongation when compared to baseline cast iron. This failure was expected due to the very nature of this dissimilar material joint.

The final type of failure observed was a shearing of the bevel in the cast iron region. This failure behavior was observed in both the U and V bevel cases. The natural shape of these bevels and the high energy input into these structures during the welding of the root pass, produces a region of high stress concentration. A significant number of the failures during this tensile testing were of this type. Simulation models developed for this research also confirmed this stress behavior.

Fracture images and macro images of the sides of these different kinds of failures are provided in Figure 63.

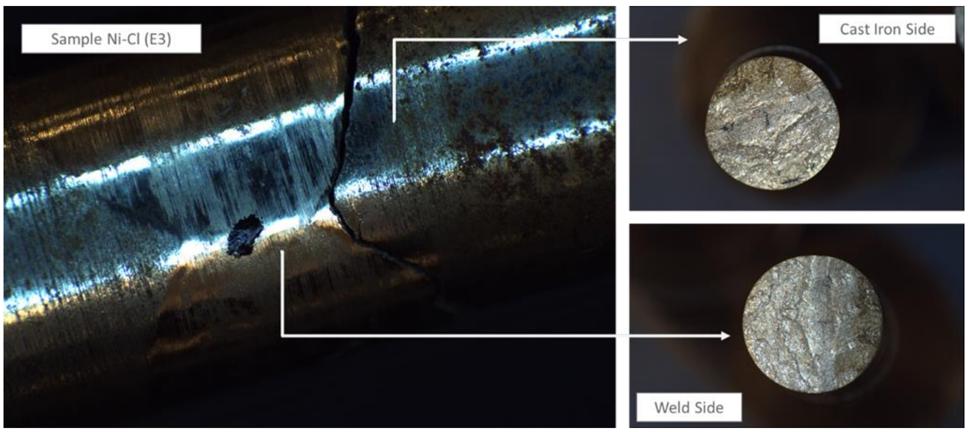

One Sided Failure

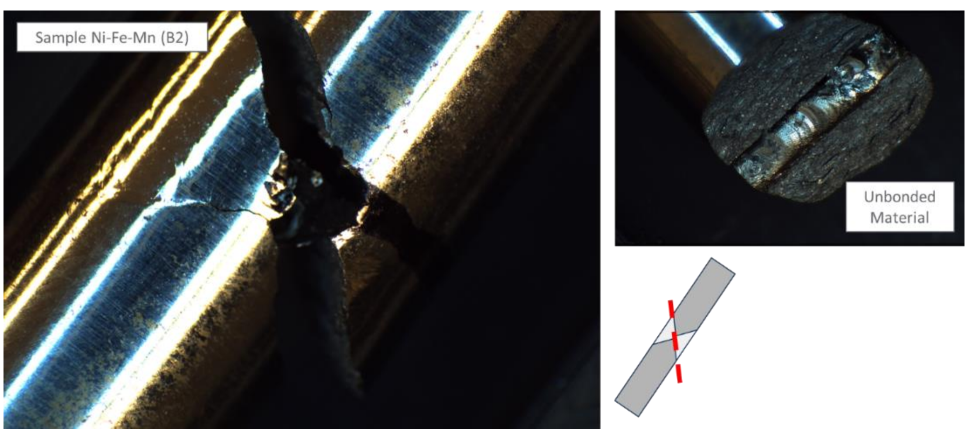

Travelling failure

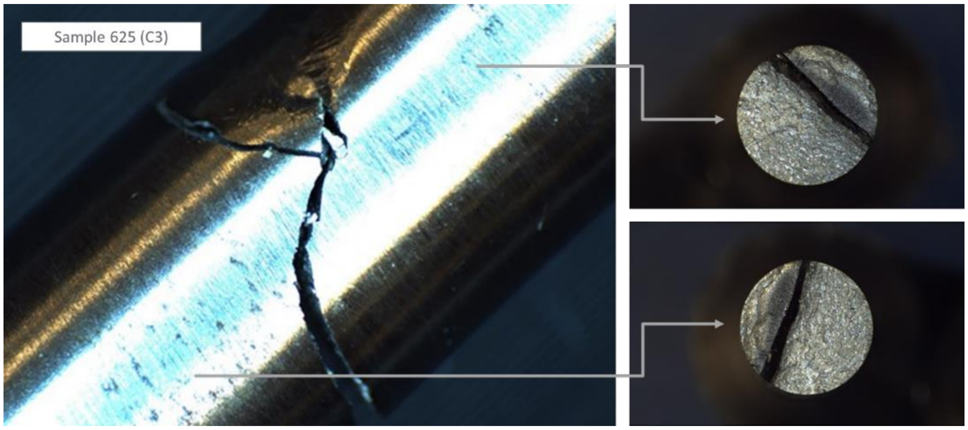

Weld-interior Partial Travel Failure

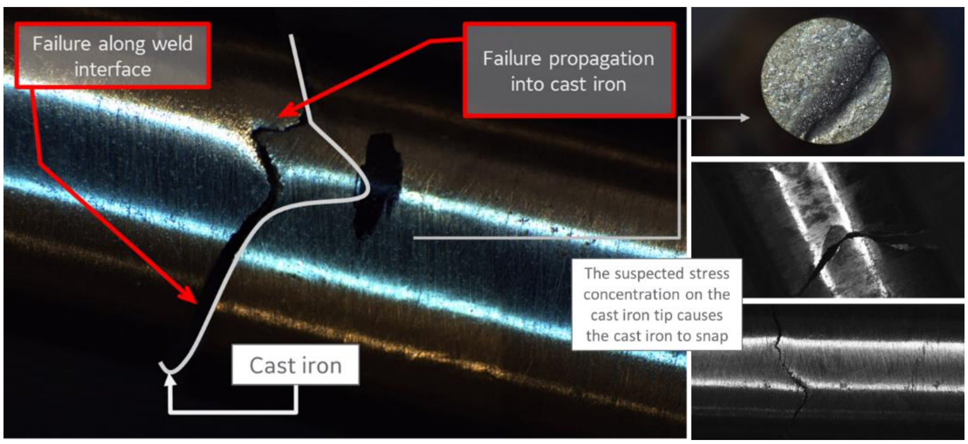

Cast Iron Partial Failure

Figure 63: Fracture surface and macro images of different types of failures observed during tensile testing.

Fatigue testing

Upon completion of the tensile testing and fractography studies, the Ni-Fe-Mn weld with cast iron was shortlisted for fatigue analysis due to its favorable strength characteristics when compared to baseline cast iron and its consistent and predictable failure modes. Defects associated with process inconsistencies were identified and corrected for to make the next set of 2 inch thick weld blocks for fatigue testing. While the weld's behavior during tensile testing is revealing, its behavior during fatigue loading is more representative of the loads that these welds would be subjected to, during end use. Therefore, their quantification and the study of the debit in fatigue performance is vital towards the qualification of the Ni-Fe-Mn weld.

A fully reversed load cycle (R=-1) was designed to populated comparative S-N curves for baseline cast iron and the Ni-Fe-Mn welds. Samples were cut and prepared as detailed in sections 1,2 and 3 of this document. A 1.5 million cycle life was assumed to be run out, although some samples were tested till 8.5 million cycles to validate the assumption. These comparative S-N curves are presented in Figure 64 and Figure 65.

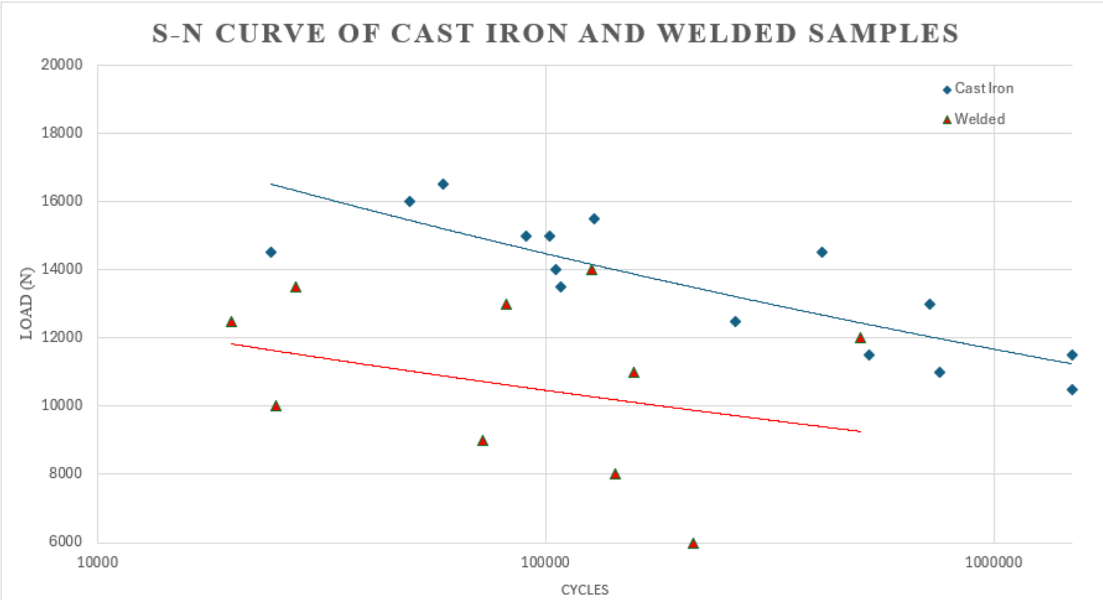

Figure 64: Log scale S-N curve of fatigue performance between baseline cast iron and Ni-Fe-Mn welded samples.

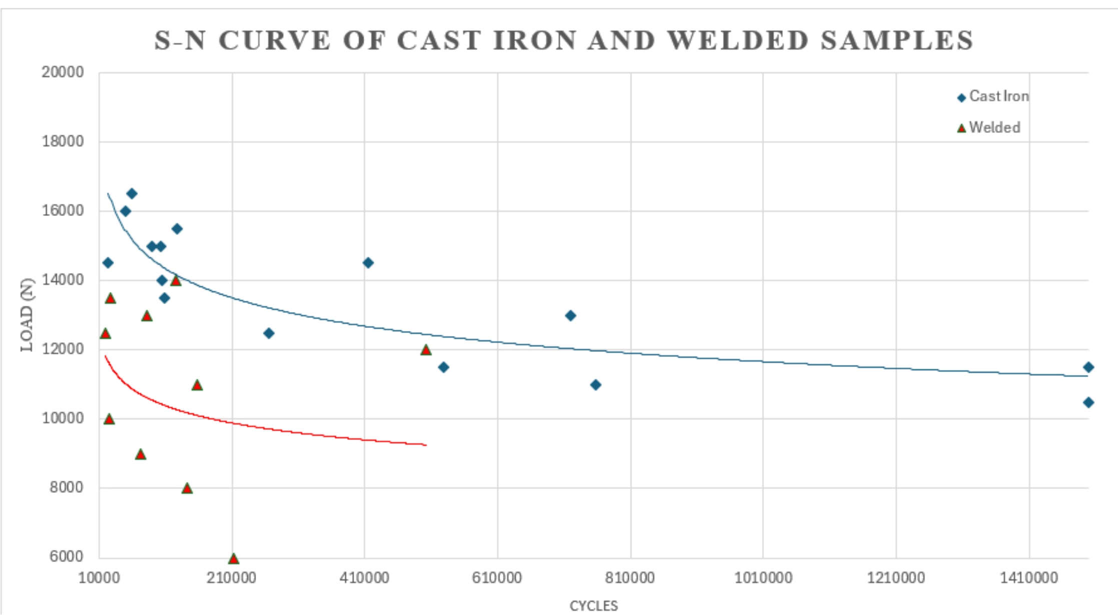

Figure 65: Regular scale S-N curve of fatigue performance between baseline cast iron and Ni-Fe-Mn welded samples.

At first glance, it can be observed that there is a life cycle and strength debit in the data observed from the welded samples when compared to the baseline cast iron. While two of the cast iron samples hit the assumed run out life cycle limit of 1.5 million cycles, none of the welded samples did, with the highest life cycle plotted at a little over 0.5 million cycles.

Having said that, it can also be observed that there is significantly higher scatter in the data from the welded samples as opposed to the cast iron. This is usually an indication of the presence of defects which adversely affect fatigue life and are being confirmed through fracture surface analyses of these samples. Samples that did not exhibit defects achieved much higher and anticipated life, while samples that did failed prematurely, with some even failing within the preload of the samples. These observations are detailed in the forthcoming sections and will be corrected for during the weld of the larger 2 inch and 4 inch sections.

Welding of Sub-article

Based on the successful of welding 1” coupons and characterization of weld performance, weld processes to scale up to larger thicknesses were pursued. There were two main challenges to scaling up the processes. Firstly, understanding the thermo-mechanical stresses generated during the welding process and the potential risks to cracking. Secondly, the process modifications to enable deep groove welding as needed by this effort.

Extensive thermo-mechanical welding simulations were pursued under this program to estimate the distortion and residual stresses from welding process. The effects of process parameters and weld coupon dimensions were estimated and reported in other deliverables. The maximum equivalent stress from the simulations is shown in Figure 66. While the overall range of stresses remains within the same range, after a certain thickness of welding the peak stress in the part was calculated to dip and increase. The thickness at which this happens was seen to vary with weld thicknesses. Additionally, the stress was seen to be concentrating along the center of the bead. While the 1” samples were fabricated without cracking, the risk of cracking while welding larger thickness samples needed evaluation.

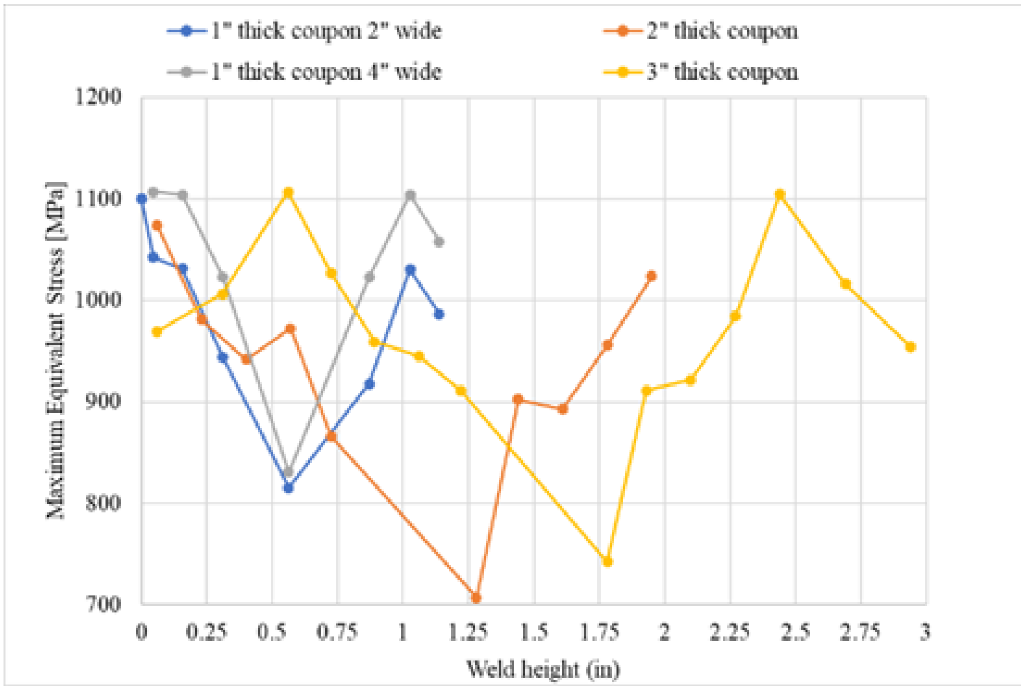

Figure 66. Maximum equivalent stresses in the welded coupons (stress values have not been validated)

In order to facilitate the deep groove welding for the large thickness specimens, modifications to the hardware and process were necessary. These changes involved modification of the torch to reduce dimensions to tackle, collision and clearance with the groove during welding. Given the larger volume of welds to be made, additional process parameters were also generated for filling the weld groove a volume.

A special GMAW torch tip was utilized to perform the larger thickness welds, a picture of the torch tip is shown in Figure 67. For larger groves, the torch needed further modification to enable collision free movement and access. Parameters such as standoff distance and inert gas flow needed significant modification to enable usage of this torch on the welder. These modifications were significantly different from the optimized setup used to weld the 1” thick coupons and process optimization trials were resumed to ensure reproducibility of the optimized process. Primary challenges to this included oxidation, and failure of open gap root pass using NiFeMn filler wire.

Figure 67. Narrow body torch used for deep groove welding.

The setup for welding the larger thickness specimens is shown in Figure 68. The setup process involved inclined deposition setup similar to the 1” thickness welds of NiFeMn, with inert gas backing for root pas welding and narrow torch body for deep groove welding. The tool path for deep groove welding was generated for alternating deposition direction to manage residual stress and distortion similar to prior welds.

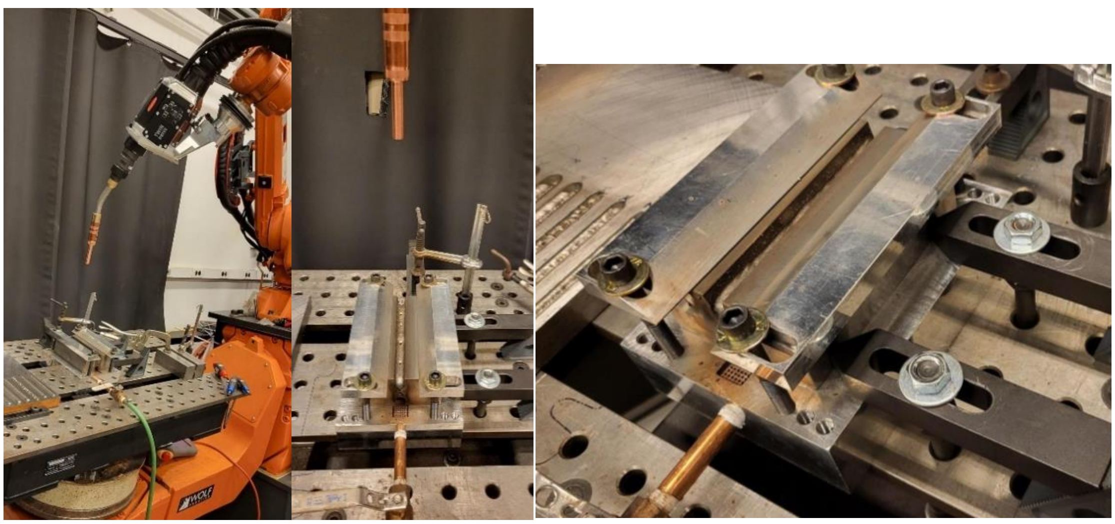

Figure 68. Setup for deposition of large thickness coupons demonstrating, angled weld setup, narrow body torch and inert gas backed fixture for butt welding.

The welding process was successfully replicated for the 2” thick weld coupons while overcoming challenges pertaining to root pass process stability and oxidation. The process of welding the 2” thick coupon involved multiple passes of deposition with alternating deposition direction. After multiple attempts, cracking across the bead center line was noticed in the welds. This cracking was observed after a total weld thickness of 1”. The outcome of cracking lines up with the simulation estimation rise in stress. Varying process parameters, such as scan speed, power and interpass temperature did not address the cracking issue. A picture of the center line cracking is shown in Figure 69.

Figure 69. Centre line cracking seen in the filler material

3.Thermo-mechanical modeling

Background:

TM welding simulations have been used to explore welding parameters and identify assembly strategies considering potential for failure and challenges encountered when the welding process is scaled up from the coupon level samples to the large-scale geometries

The first stage of the evaluation has been to perform TM simulations which are high-fidelity for the small-scale cast-iron weld coupons to identify the potential problems encountered when the coupon trials are scaled up from 1” to 2” and eventually to 3” thick samples. The results from the simulations would yield the stress contour along the coupons along with distortions of the coupons after the welds are performed to see the areas of high stress concentration which would likely be the areas of failure in the sample.

After performing the high-fidelity simulations and assessing the potential risks of scaling up the samples, a low-fidelity simulation has been performed on large scale model. The model attempts to replicate weld assembly of a representative wind turbine geometry. The TM modeling results from this work indicate potential areas where we would observe failure in the process and how it could be addressed.

Coupon and Weld Bead Design:

The initial geometry of the coupons was based on the welding optimization process studies where the coupon dimensions used in the process had been taken as the guideline to design coupons for simulation. The weld coupon taken for the simulation were 6” long, 1” high and 2” wide, consistent with the weld coupons considered for the weld optimization study. The geometry has been shown in Figure 70. The geometry design for the 1” based weld beads were calculated based on the wire feed parameters that were logged during welding. This was done to match the volume of weld bead with the actual welding process. Replicating the optimized welding processes, it has been determined that the total number of passes to simulate the 1” weld would be 10 passes like the optimized welding process. The welding torch path was alternated between the top side of the U-groove and bottom as detailed by the alternating weld pass numbers on each side of the U-Groove in Figure 70.

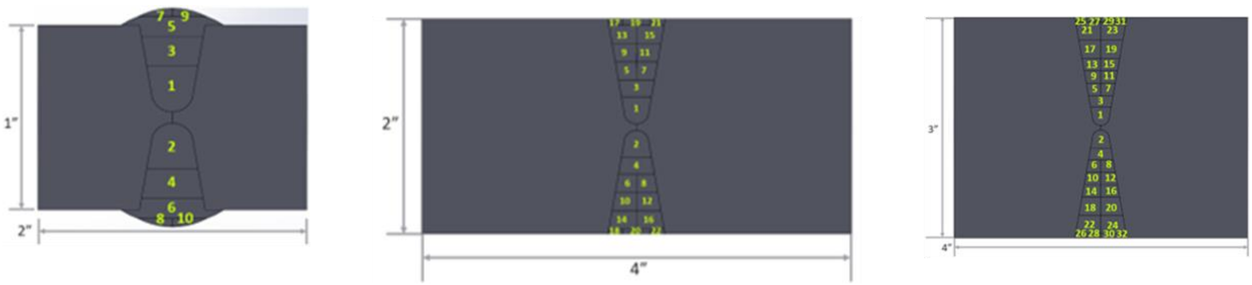

Figure 70: (Left) Cross-section view of the 1", 2” and 3” weld coupon.

A unit cell approach has been used to evenly scale up the geometry from 1” to 2” and 3” thick weld coupons for the weld bead design. The root pass and the fill pass 1 from the 1” weld coupon has been carried to both the 2” and 3” thick weld coupons. The cap pass has not been extended beyond the height of the weld coupon for the 2” and 3” thick weld coupons. For the 2” thick weld there are 22 weld passes and for 3” thick weld there are 32 weld passes (see Figure 70).

Coupon and Weld Bead Mesh:

The coupon and weld bead geometry mesh were generated using Hypermesh software developed by Altair. This tool was chosen due to its flexibility for designing an optimized mesh for the application. Along the x, y and z axes the element size has been varied to reduce the computational time and maintain a balance between accuracy and efficiency. The mesh generated for the TM simulation have been reviewed and approved by Hexagon corporation that develop SW software. In multi-body TM simulation, one of the key challenges to meshing is to maintain continuity in mesh as it transitions from weld bead to base metal. SW software uses Linear element type whose derivatives are discontinuous and if there is a scenario of discontinuity in the mesh between two different geometries, this causes nonphysical jumps in results. Ensuring continuity was one of the primary constraints during mesh design and this created limitations around having a finer mesh near the weld bead and base material compared to the portion of the base material that was further away from the welding process.

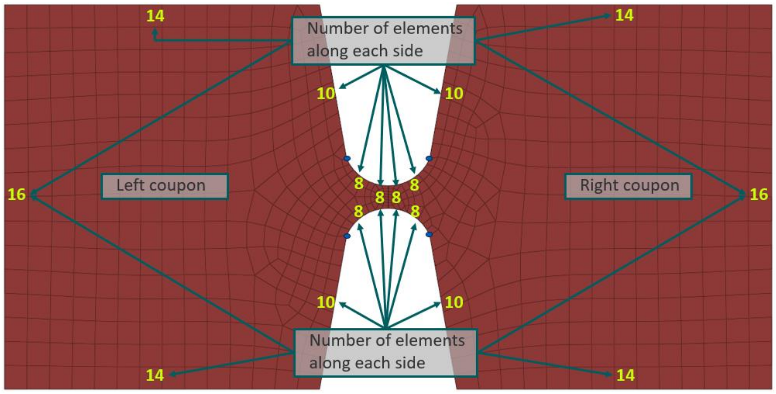

Figure 71: Coupon mesh details.

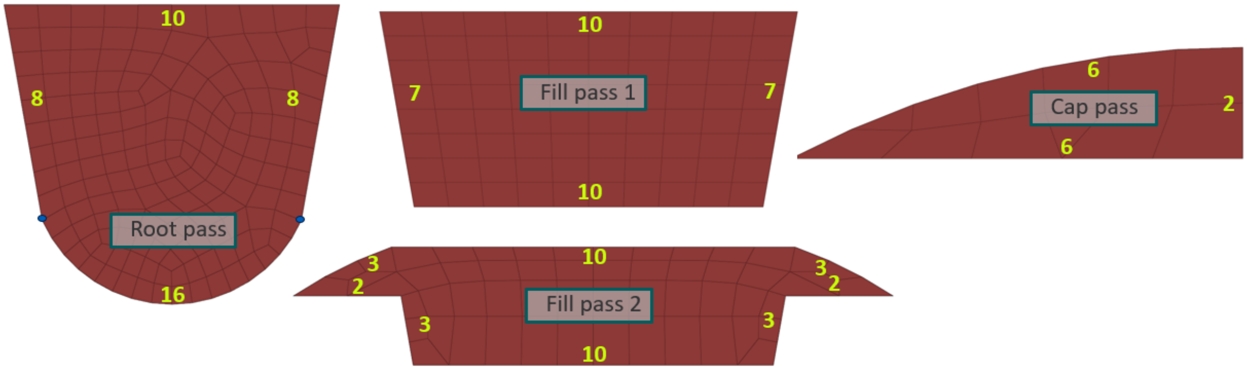

Figure 72: (Left) Root pass mesh, (center top) Fill pass 1 mesh, (center bottom) Fill pass 2 mesh, and (right) Cap pass mesh.

Table 2: Weld pass element size details

Weld Pass Number	Classification	Element size (mm)
1 2	Root pass	0.54
3 4	Fill pass 1	0.64
5 6	Fill pass 2	0.89
7 8	Cap pass left	0.74
9 10	Cap pass right	0.74

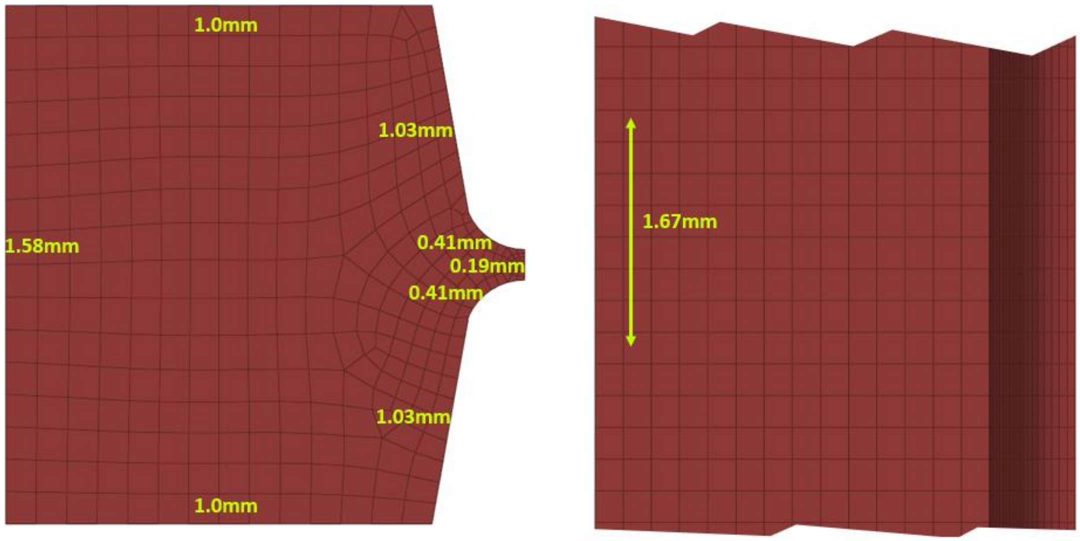

Figure 73: (Left) Coupon element size along x-y direction, and (right) element size along the z axis length of the coupon cut section.

When we see the number of elements used for each edge for the weld coupon shown in Figure 71, we can observe that the element size used is not constant throughout the 3D geometry. The variation in the element size across the geometry is detailed out in Figure 73. The element size is small along the weld beads and coarsens out away from the weld bead. Also, along the length of the coupon the element size is coarse. In Table 1 the average element size for each weld pass has been explained along the x-y direction (cross-section of the weld). The element size along the length of the weld is 1.67mm which is the same for the weld coupon.

Simulation Setup

Process Setup:

The process setup for the high-fidelity model along with the heat source setup have been explained in detail in prior reports for Deliverable 3.2. The process setup is similar for the 2” and 3” thick simulations. The heat source values are scaled up for the 2” and the 3” thick coupons. When the model is scaled up to the large-scale simulation a low-fidelity thermal cycle model has been used that is explained in a later section of this report.

Process Parameters:

The heat source process parameters current, voltage and efficiency of the weld is based on the actual welds that were performed on the 1” thick coupons. The voltage and current settings along with the wait times between the deposition of the weld beads are consistent with the actual welding process.

In Figure 74 the heat source parameters for the root, fill and cap passes have been highlighted for the 1” and 2” thick weld coupon welds and are compared with the heat source process parameters from the weld optimization task.

Tool Path:

For the simulation process the welding tool path is a straight line along the length of the weld. The welding direction alternates between the top side of the U-groove and the bottom. Furthermore, the start and end points on a given side were also alternated. This method has been implemented for the 1” thick weld coupon and will also be consistently implemented to the 2” and 3” thick coupons. This process of alternating the paths has been done to simulate balance welding process.

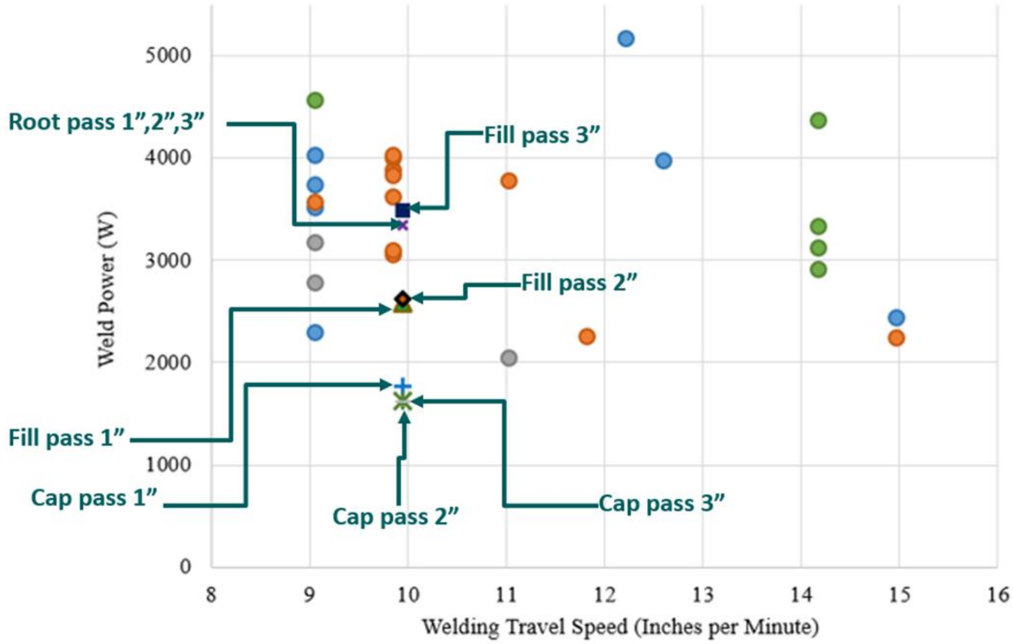

Figure 74: Heat source process parameters for the root, fill and cap passes for the 1",2", and 3" thick weld coupon.

Thermal Strain Model for Large Scale Simulation:

Thermal cycle is a thermomechanical low fidelity simulation that has been used to perform the TM simulation for the large-scale model. The thermal history of the data that has been generated from the peak temperature values for the high-fidelity simulations for the 2" and the 3" specimen is taken as the input for the thermal cycle model. The thermal data from the high-fidelity coupon simulations is used as the input for the large casting simulation. This option is chosen for the large-scale model to balance between accuracy and computational efficiency. The mesh size is the driving factor and for a large model the mesh though coarser in terms of the element size would still generate a lot of elements that would increase the computational time exponentially.

Results and Discussion

The results that are going to be discussed in this section are solved using the TM analysis using SW software. The TM analysis is done by fully coupled analysis of thermal component and the structural component. The stress contours that are being shown in this section are calculated after performing the coupled analysis. A fully coupled analysis in this case is an analysis where the thermal equations and the structural equations are simultaneously solved during the simulation. The coupling of the thermal and the structural analysis are happening in incremental steps. Since, SW software is a FEA based software the convergence of the solution at the end of each incremental time step is dependent on the mesh size being used. Further in this work since the geometry of the weld coupon and filler materials are complex due to curve and bevel angles.

Initial Simulation Setup:

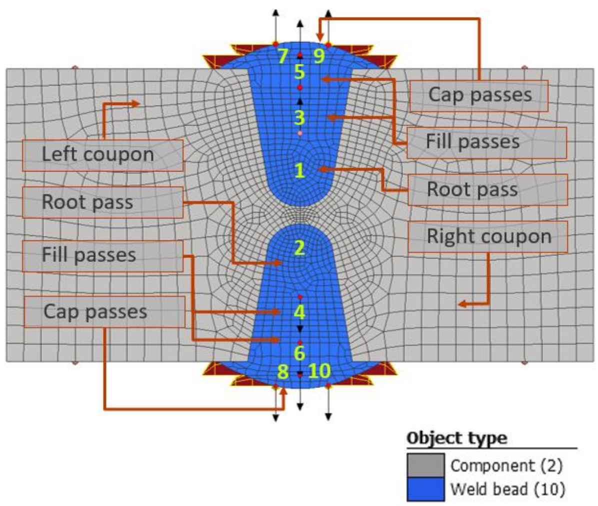

Figure 75: Mesh setup with the filler material at the start of the simulation for the 1” thick coupon.

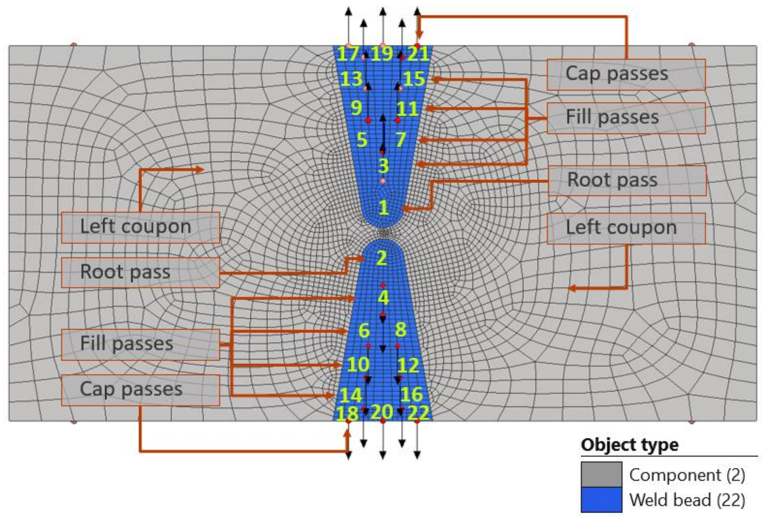

Figure 76: Mesh setup with the filler material at the start of the simulation for the 2" thick coupon.

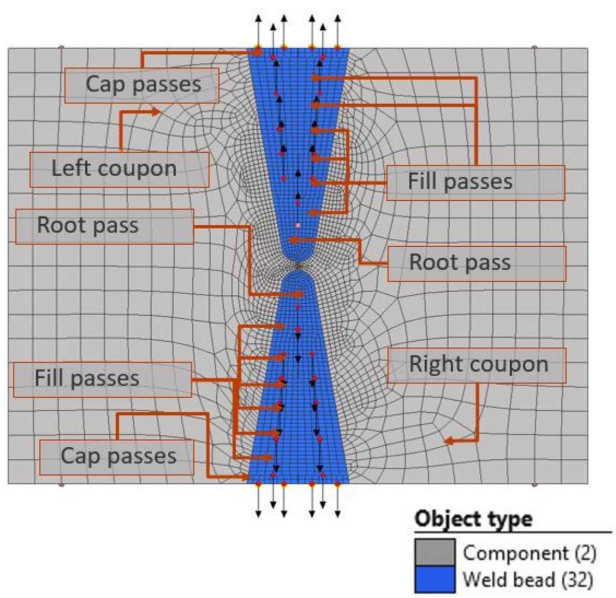

Figure 77: Mesh setup with the filler material at the start of the simulation for the 3" thick coupon.

In Figure 75,Figure 76, and Figure 77 the initial simulation setup for the 1”,2” and 3” thick coupons have been displayed. The root pass and the first fill passes have the same geometry as the weld coupons have been scaled from the 1”,2” to the 3”. The width of the filler passes for the 2” thick weld coupons and the 3” thick weld coupons have been split to calibrate the heat input per unit volume to be consistent with the 1” weld coupons. In the 1” thick coupon there are two fill passes, when the coupon is scaled up to 2” thick coupon then we have 4 fill passes and in the 3” thick coupon there are 6 fill passes. The root pass is shared between all the weld coupons from 1” thick to 3” thick coupon.

Normal Stress along weld bead length:

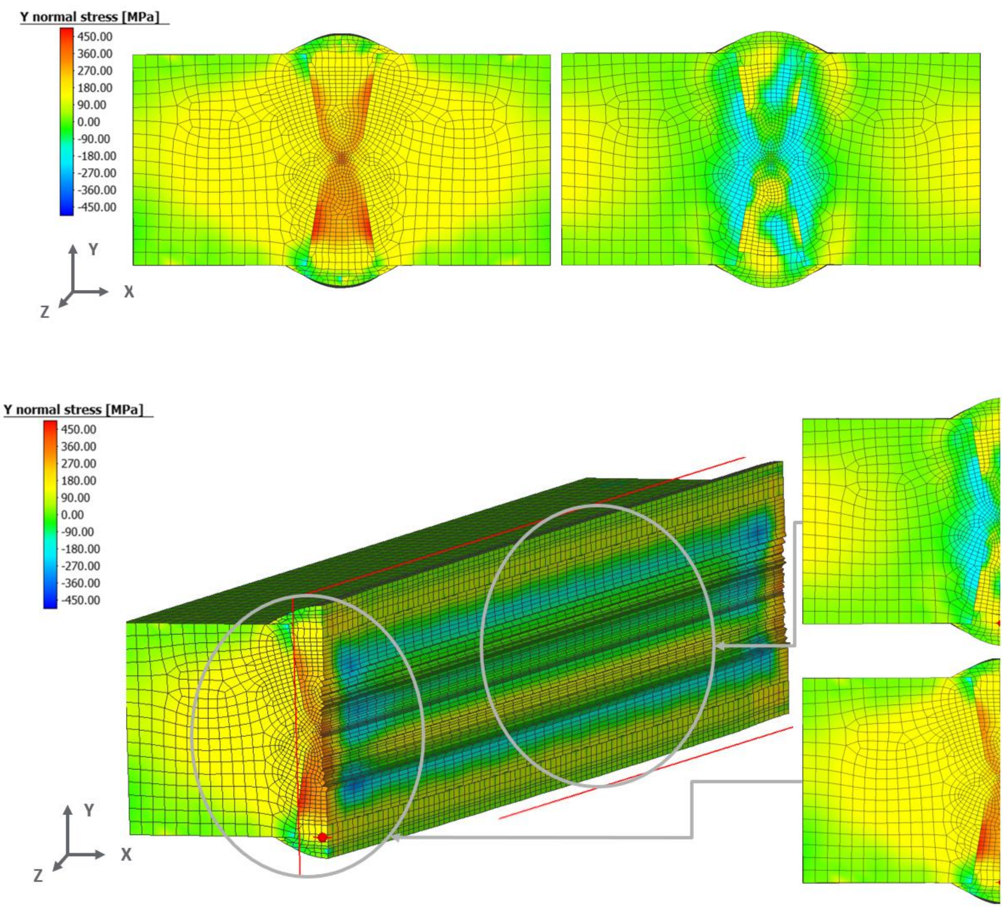

Figure 78: (Top left) Normal Stress along the thickness of the coupon at the edge for a 1" coupon, (top right) Normal stress along the thickness of the coupon at the mid span for a 1" coupon, and (bottom) normal stress along the thickness of the weld coupon. (Stresses are not validated. Results are for qualitative analysis)

The Figure 78 shows the normal stress along the Y direction or along the thickness of the 1” thick coupon. When we take a closer look at the normal stress distribution, the stress value is higher at the edge of the weld coupon when we compare to the normal stress distribution at midspan or at 3” along the length of the weld.

Distortion along the weld bead height for the 1” thick coupon:

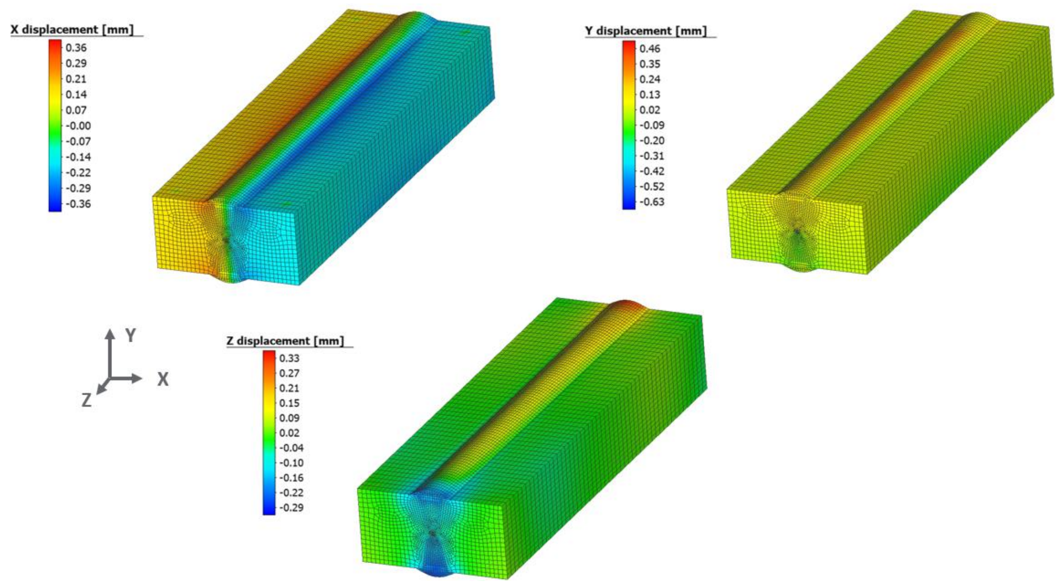

Figure 79: Displacement plot along the x, y, and z directions for the 1" thick weld coupons. (Stresses are not validated. Results are for qualitative analysis)

In Figure 79 the distortion or the displacement has been measured at the end of the simulation along the x, y, and z directions. When we compare the displacements, we do observe that they are low but along the y direction or along the height of the weld the value is a bit higher than along the x and z directions. Further when we compare the displacement compared at the clamped state between both simulation and experiments for the 1” weld coupon they are in good agreement, the displacements or the distortion is low.

Stress analysis for the different thickness coupons:

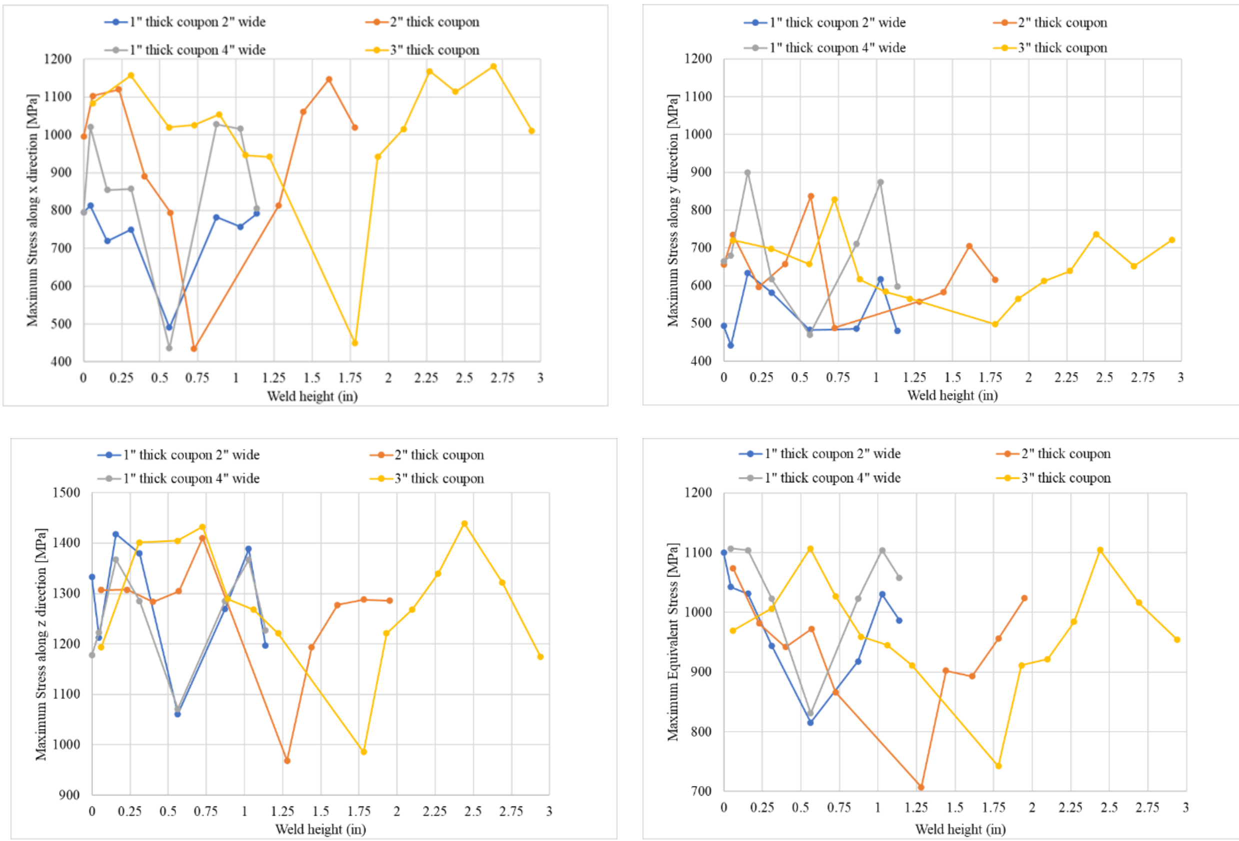

Figure 80: (Top left) Maximum normal stress in x direction, (top right) maximum normal stress along the y direction, (bottom left) maximum normal stress along the z-direction, and (bottom right) maximum equivalent von-mises stress for all the coupons. (Stresses are not validated. Results are for qualitative analysis)

In Figure 80, the maximum normal stress along the x, y, and z directions along with the maximum equivalent stress has been plotted along the thickness of the weld from 1” thick coupon with 2” width, 1” thick coupon with 4” width, 2” thick coupon, and 3” thick coupon to observe the evolution of the stress as the coupons are scaled up. The stress value has been captured at the end of each weld pass and at the end of the cooling cycle before the beginning of the deposition of the next pass. From the trend of the stress components along the height of the weld, the maximum normal stress is observed along the z-direction or along the length of the weld compared to the other stress components. The trend in the stress components as the weld coupons are scaled up from 1” to 2” and 3” is preserved and we do not see a significant change in the trend of the stress evolution as the coupons are scaled up. This helps determine that the scaling up of the coupons itself would not cause a huge difference in the failure points of the coupon. The stress is seen to rise with thickness, dip and rise again. The same trend is seen across the different thicknesses.

Normal Stress along the weld bead height for 1" thick and 2" wide:

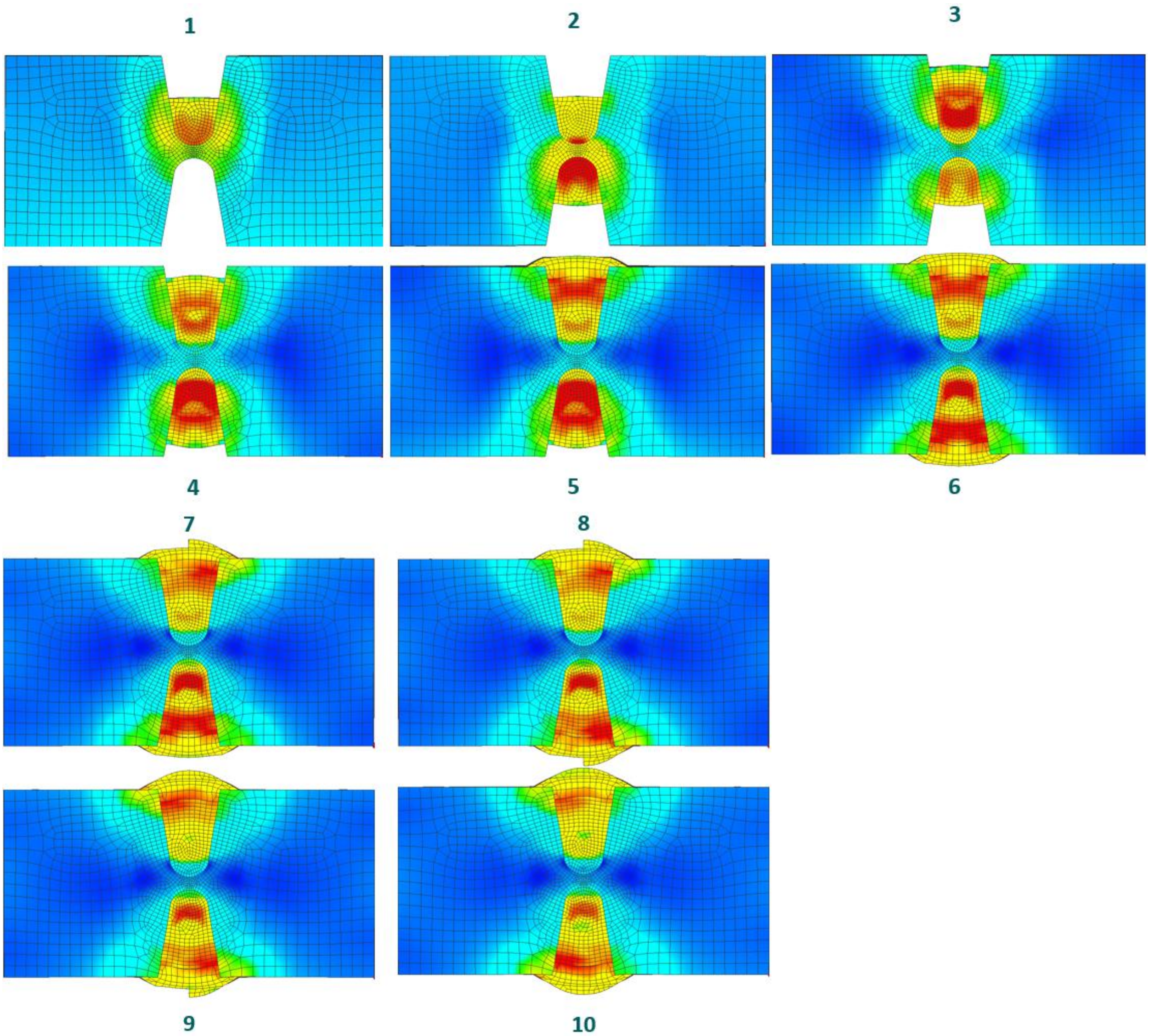

Figure 81: Normal stress along the length of the weld coupon or along the z direction, snapshots taken at midspan of the weld coupon for 1" thick coupons. (Stresses are not validated. Results are for qualitative analysis)

Figure 81 shows the normal stress distribution along the z direction or along the length of the weld. From the top to bottom in the image we show the stress contour along the weld coupon and the weld bead as the weld passes are deposited from the first pass to the final weld pass 10. The contour has been studied at the midspan length or at 3” along the weld length. The contour is taken at the end of the weld process for each pass and at the end of the cooling cycle.

Normal Stress along the weld bead height for 2” thick coupon:

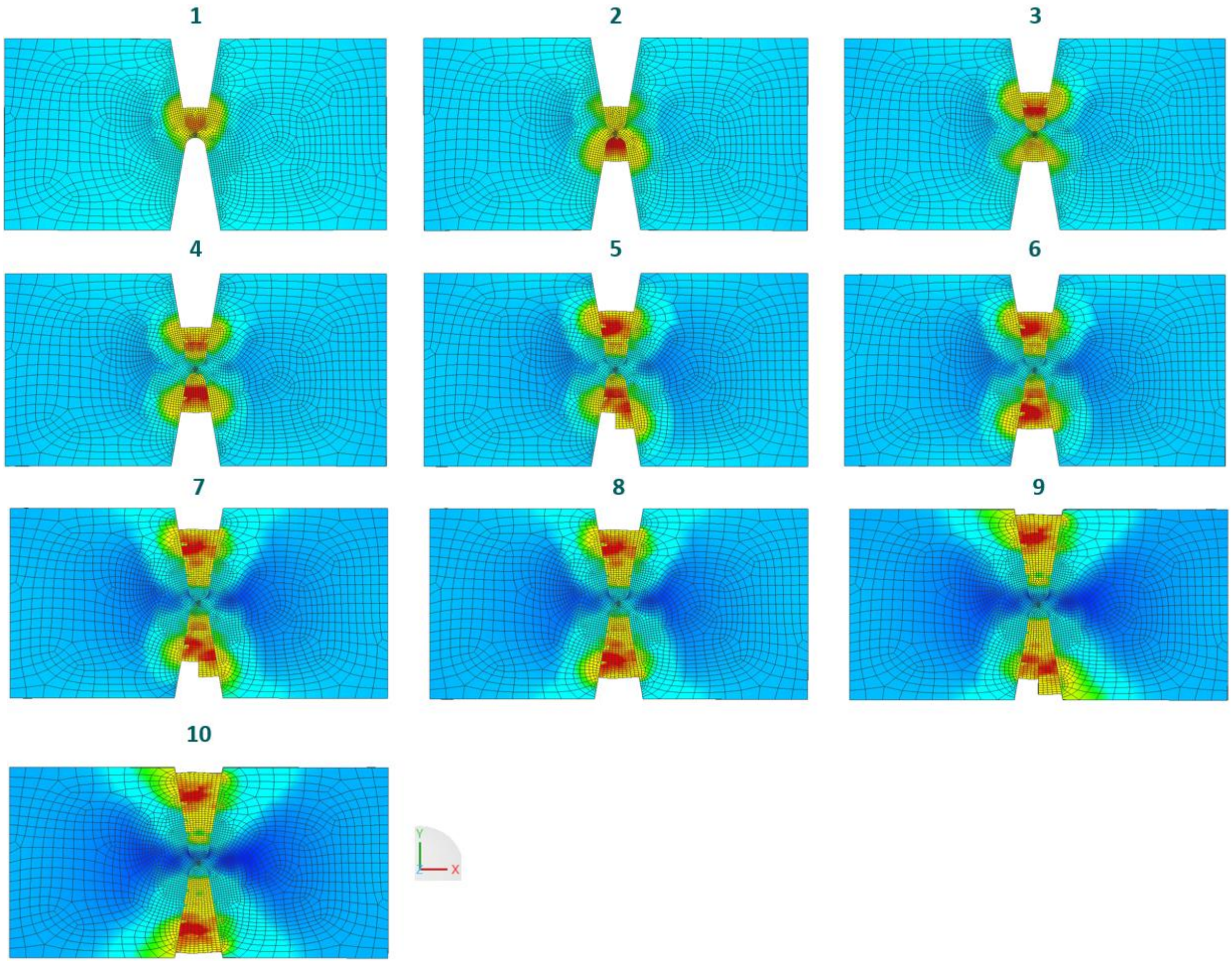

Figure 82: Normal stress along the length of the weld coupon or along the z direction, snapshots taken at midspan of the weld coupon for 2" thick coupons. (Stresses are not validated. Results are for qualitative analysis)

Figure 82 shows the normal stress distribution along the z direction or along the length of the weld. From the top to bottom in the image we show the stress contour along the weld coupon and the weld bead as the weld passes are deposited from the first pass. The contour has been studied at the midspan length or at 3” along the weld length. The contour is taken at the end of the weld process for each pass and at the end of the cooling cycle.

Normal Stress along the weld bead height for 3" thick coupon:

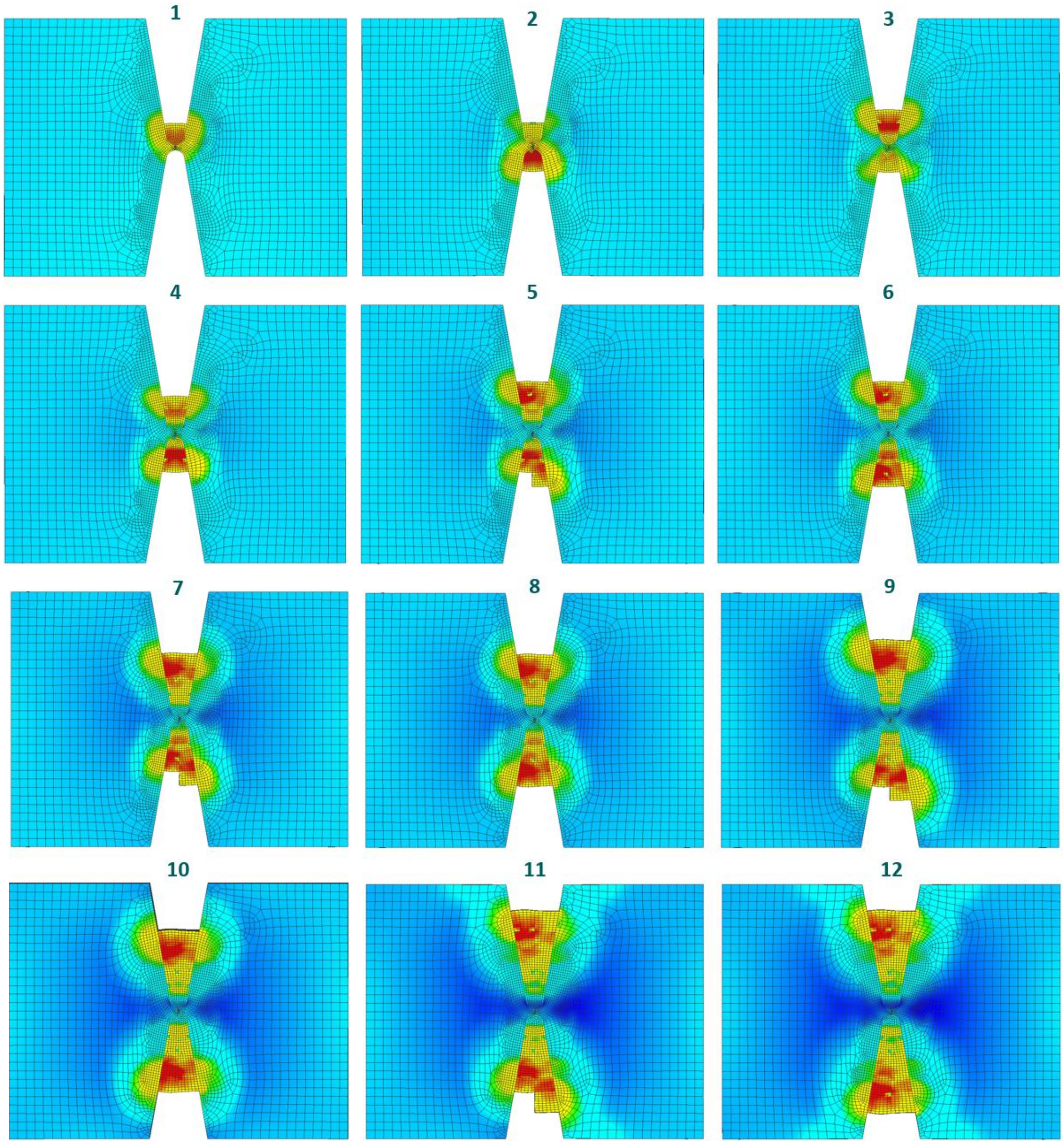

Figure 83: Normal stress along the length of the weld coupon or along the z direction, snapshots taken at midspan of the weld coupon for 3" thick coupons. (Stresses are not validated. Results are for qualitative analysis)

Figure 83 shows the normal stress distribution along the z direction or along the length of the weld. From the top to bottom in the image we show the stress contour along the weld coupon and the weld bead as the weld passes are deposited from the first pass. The contour has been studied at the midspan length or at 3” along the weld length. The contour is taken at the end of the weld process for each pass and at the end of the cooling cycle.

Normal Stress along the weld bead height for 1” thick and 4” wide:

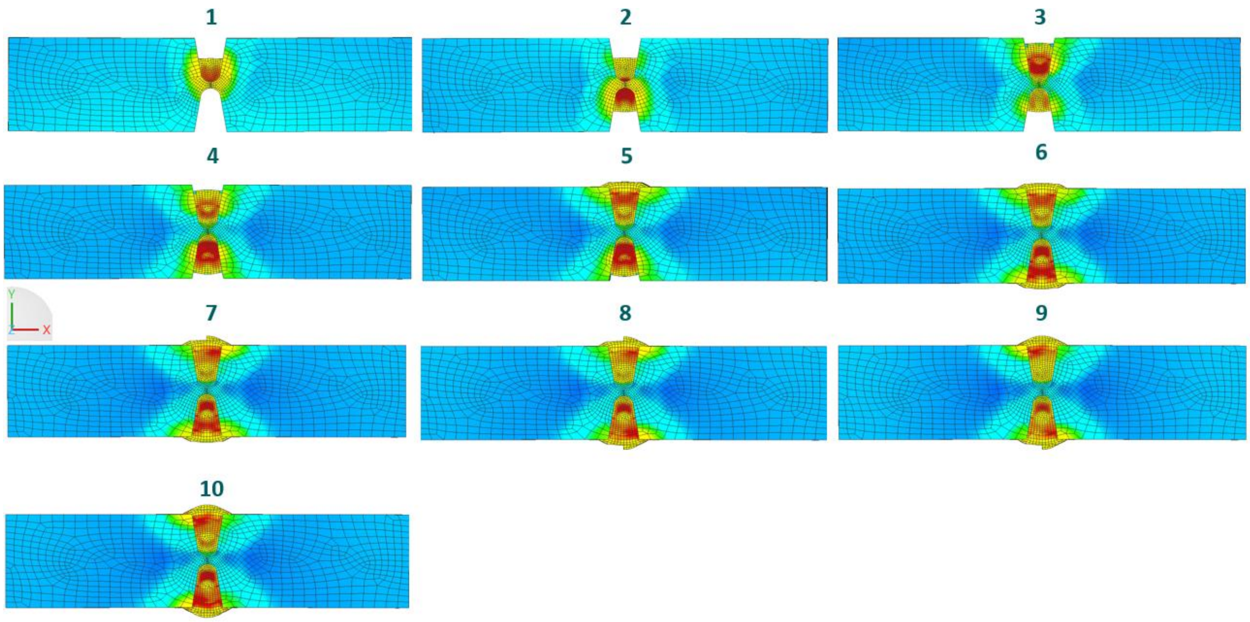

Figure 84: Normal stress along the length of the weld coupon or along the z direction, snapshots taken at midspan of the weld coupon for 1" thick and 4” wide coupons. (Stresses are not validated. Results are for qualitative analysis)

Figure 84 shows the normal stress distribution along the z direction or along the length of the weld. From the top to bottom in the image we show the stress contour along the weld coupon and the weld bead as the weld passes are deposited from the first pass. The contour has been studied at the midspan length or at 3” along the weld length. The contour is taken at the end of the weld process for each pass and at the end of the cooling cycle.

Large Scale Low Fidelity Simulation:

In this work, a low fidelity thermal cycle model has been implemented to simulate a large-scale model which is a rotor of a wind turbine. The rotor has a diameter of 6m, a height of 1m and has a wall thickness of 0.097m. This simulation is tasked to simulate a large-scale casting welding process. The rotor is sectioned into 4 sectors and is welded with 4in thick welds that are split into 2 passes that are 2” sections. Due to the complexity and load it would put on the computational resources, the thermal cycle simplified model has been implemented using the data that has been generated through the coupon welding simulations. The details about the thermal cycle model have been explained in the simulation setup section.

A total of 16 passes have been used to weld the different sectors of the large component. Two

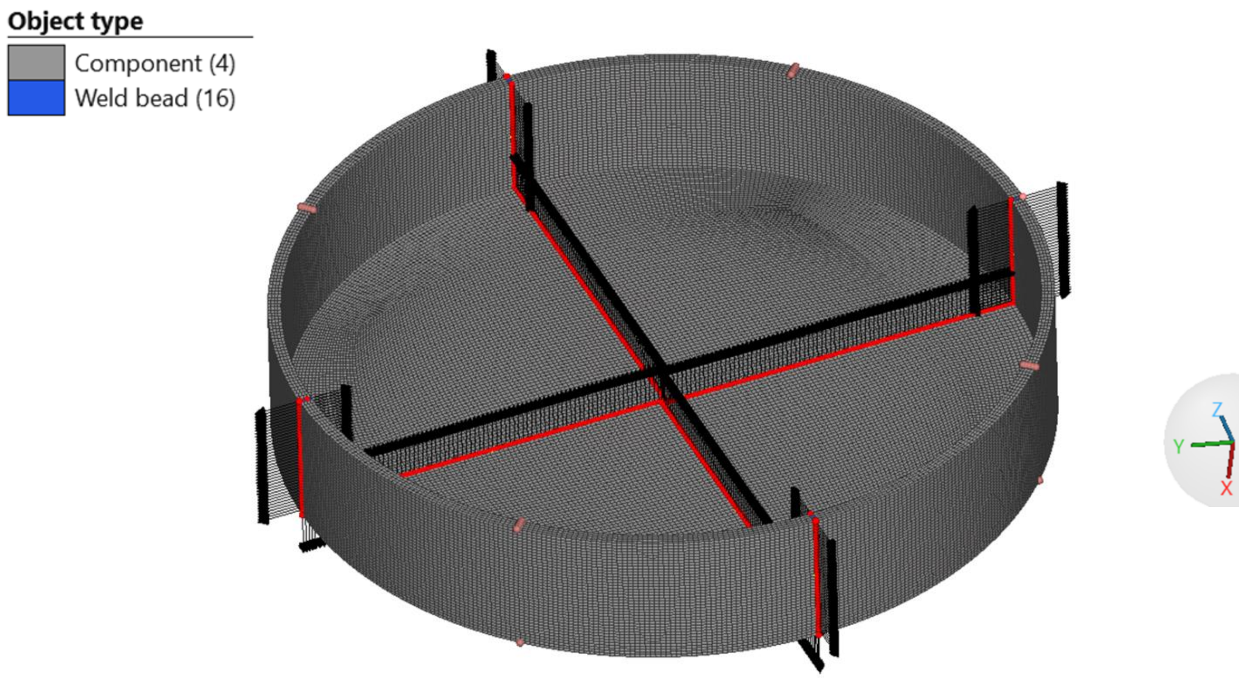

Figure 85: Isometric view of the rotor with the weld passes.

passes along the rotor wall and two passes along the base of the rotor. Balance welding procedure like the weld coupons has been used in this work. The weld passes have been deposited from the outside of the rotor to the inside. Figure 85 shows the mesh of the rotor along with the trajectories. To discretize the geometry a total of 223056 nodes and 172800 elements have been used. Like the weld coupon mesh shown in the earlier sections the mesh is a mapped mesh that has been used to discretize the circular geometry.

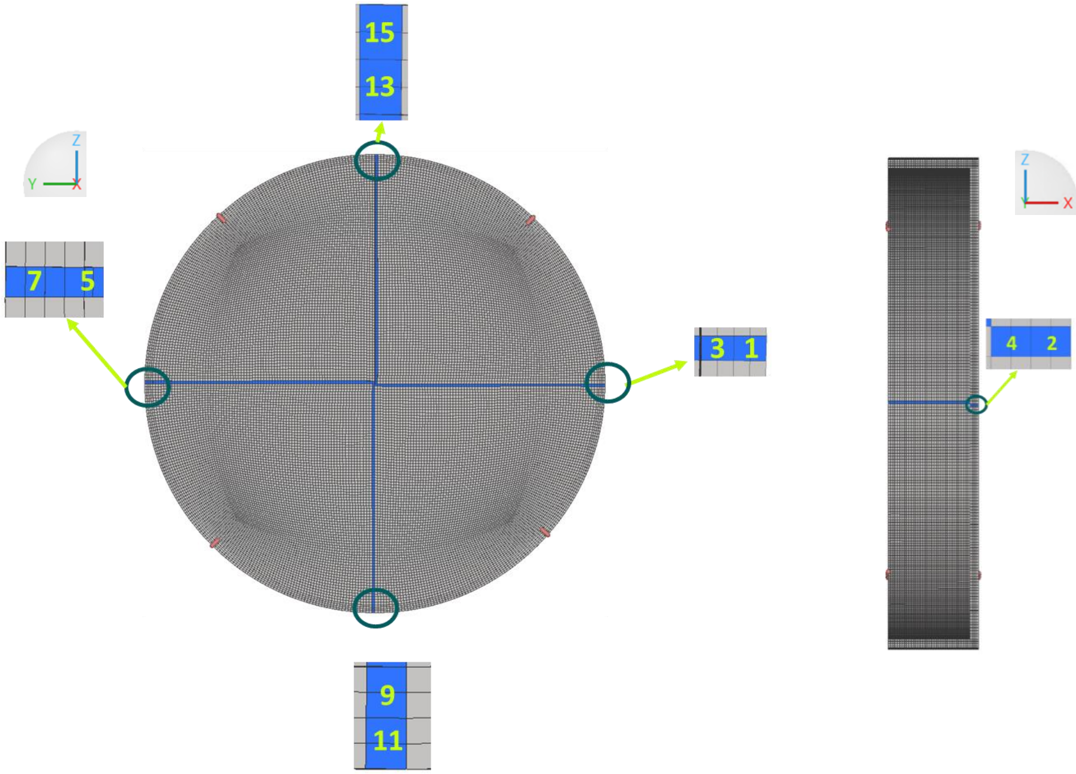

Figure 86: (Left) Shows the top view of the rotor with the weld pass along the wall and (right) show the side view of the rotor with the weld pass along the base.

In Figure 86 the top and side view of the rotor is shown with the weld passes to join the 4 different sectors of the rotor. All the even passes are along the base of the rotor and the odd weld passes are along the height of the rotor.

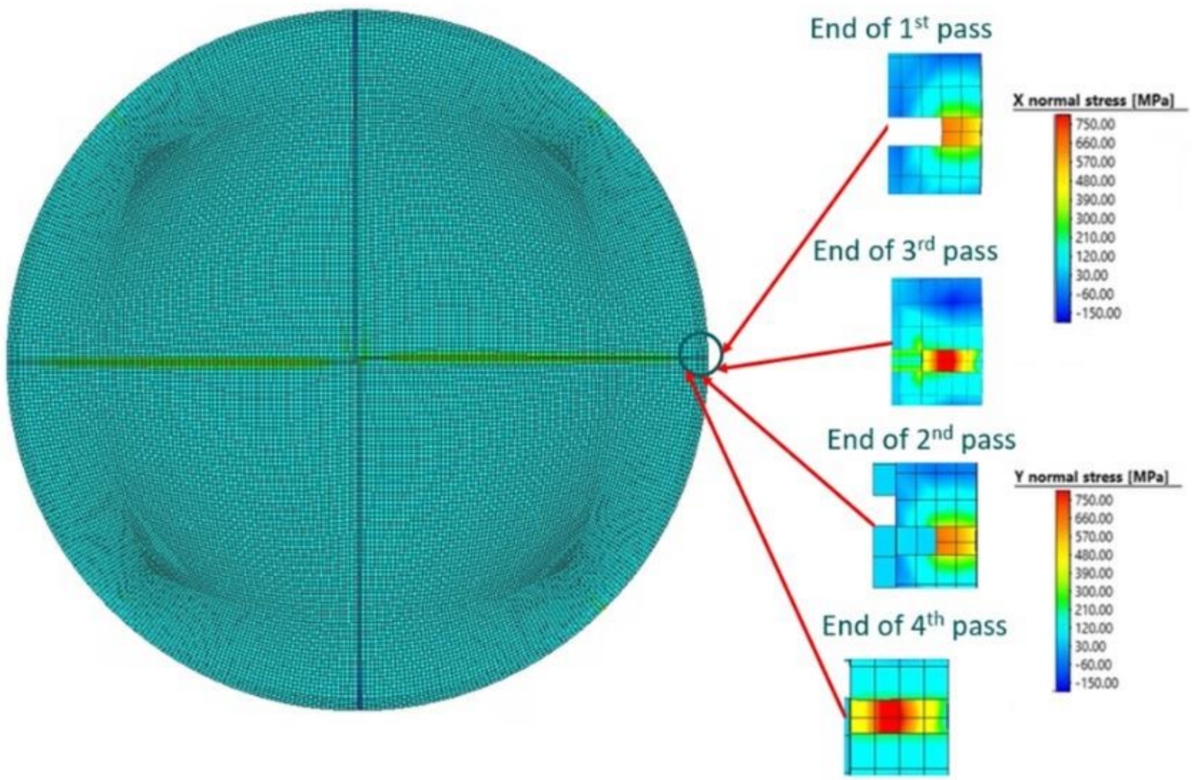

Figure 87: X normal and Y normal stress for one sector of the rotor at midplane along the base and wall. (Stresses are not validated. Results are for qualitative analysis)

In Figure 87, the normal stress along the length of the weld pass for both the rotor wall and base has been shown. The stress is plotted along the 180-degree orientation of the rotor when viewed from above. When we are evaluating the stress along the length of the weld along the rotor wall then we must consider x-normal stress and when we are evaluating the stress along the length of the weld along the rotor base then we must consider the y-normal stress. When we take a closer look at the stress contour along as the passes are deposited, we see that the peak stress at the end of the second pass is at the interface between the first and the second pass. This contour is consistent with what has been observed in the coupons. The 4th pass is at the end of the welding process at the midplane along the length and the maximum stress concentration is in between the interface of the weld passes.

Distortion Measurement:

In this work the distortion that is accumulated as the welds are made to join the sections of the rotor is discussed in this section. As the welds are made from the root pass to the cap pass, the rotor is clamped using a fixturing method that prevents the part from moving as the welds are being done but after the welding process is completed the fixtures are removed, the thermal strain that is accumulated within the part is dissipated and the part distorts which help us determine the amount

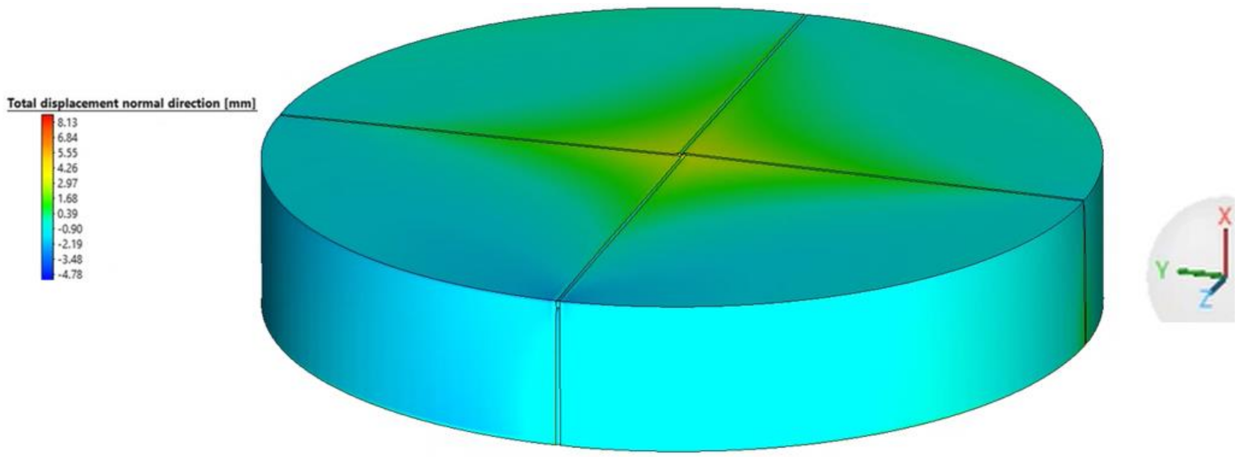

Figure 88: Total distortion in the part at the end of welding.

the part would deform and how we must compensate for it. A total of 16 welds are made and the part is cooled down as the fixture is removed to determine the distortion in the rotor after the final part is made.

In Figure 88 the distortion contour of the rotor is shown, we can observe that the maximum distortion happens at the edges of the 4 sections that are welded together. This is due to the accumulation after the welding process, all the welds intersect at the center region of the rotor which is the location where we are observing the maximum distortion.

Summary of findings:

From this work we have calibrated SW software parameters to match the parameters being used for the 1” weld coupon to understand the variations in results and accordingly recalibrate the material properties and other parameters in SW software to match the data from 1” welds. Using the parameters of the 1” coupon, the parameters were scaled up with one key factor being maintain the same heat input that was used in the 1” weld coupons to using similar heat input for the 2” and the 3” weld coupons.

One component of the simulation that we have used to validate with experiments is the stress along the length of the weld at the midplane region. The midplane is selected so that edge effects are not considered in the simulation data. Based on the results we have observed the stress concentration regions to be close to the interface of the weld bead and the base metal and towards the side of the weld bead. The stress concentration regions as the new weld beads are deposited follow a profile that is like the failure mode that has been observed during testing. The behavior has been found to be similar for the 2” thick and 3” thick section coupon weld simulations. Further, we have also observed that the stress concentration regions are near the interface between each weld beads.

From experiments we have found that when deposit the welds beyond the 1” point we observe cracking which is consistent with the stress trend that we are observing for the 2” weld coupon. There is dip at point just before the ¾” region and the stress peaks afterwards. This can be attributed to the thermal cycle load that the welds are experiencing after each cooling cycle hence in the experiment we see cracking that limits the scalability of the simulations to larger thicknesses.

For the large-scale rotor simulation, a low fidelity thermal cycle model has been used instead of the high-fidelity simulation that has been run for the smaller coupons. This approach has been used to simulate the large-scale models to have a balance between accuracy and efficiency. Given the number of elements used and the scale of the model running a high-fidelity model would take up a lot of computational resources. The accuracy of the approach has not been compromised and this can be seen in the results of the large-scale model where we have seen the dominant failure mode for the 4” thick welds to be at the interface between the welds.

4. Conclusion

The development of a qualification requirement document and a coupon-level testing plan for the welded assembly of cast iron components has addressed a significant gap in existing standards and design guides. Through a collaborative effort involving GE Vernova Advanced Research, DNV-G L, and Missouri University of Science and Technology (MST), the project has made substantial progress in establishing performance and reliability metrics for assessing and qualifying welding processes for cast iron.

Key achievements and findings include:

- Development of Qualification Requirements:

- A comprehensive review of existing standards for welded structures and cast iron components was conducted to draft a new requirement summary. This summary identifies necessary performance and reliability metrics for assessing and qualifying welding processes for cast iron, providing a foundational framework for future standards. A detailed testing plan was developed in collaboration with DNV and MST to analyze the mechanical properties and performance of welded cast iron samples. This plan will be implemented using samples created in Task 2 of the program, providing essential data for the qualification of welding processes.

- Welding Process Optimization:
    - Gas Metal Arc Welding:

GMAW processes have shown more consistent success across various weldment designs and optimized parameters for 1” thick cast iron welds. Successful procedures and parameters have been established for single-material welds and a single multi-material weld (Double U Groove with Pure Nickel and Mild Steel). The welding process for 1" thick welds was also scaled up to >2" thick welds, requiring hardware and process modifications. Despite these efforts, cracking was observed at intermediate thicknesses, aligning with simulated stress rise. Varying process parameters such as scan speed, power, and interpass temperature did not fully address the cracking issue, indicating the need for further research and optimization.

- Laser-Wire Welding:

LBW has presented challenges, particularly with cracking in the cast iron base material for weldments greater than 0.25" in thickness. Thermo-mechanical modeling and laser-based preheating are being explored to reduce thermal stresses and improve weld integrity. These methods show promise but require further investigation and optimization.

- Characterization and Testing:

Minimizing the HAZ and ensuring defect-free welds are key traits for successful optimization. The presence of cracks or other defects has been identified and will guide further process improvements. Mechanical characterization, including static tensile and fatigue testing, has been performed on welds made with different candidate filler materials. While multiple candidate systems were tested for tensile properties, only NiFeMn-based welds were selected for fatigue testing based on their yield and ultimate strengths. The testing revealed a significant drop in life and strength capability, driven by defects arising from process instability.

- Thermo-mechanical Numerical Modeling:

Thermo-mechanical (TM) numerical modeling using Simufact Welding (SW) has been conducted to simulate the welding processes. These simulations have helped predict potential failure regions, risks, and challenges, particularly for U-Groove cast iron coupons and a large-scale wind turbine rotor model. The results will inform the optimization of welding parameters and the design of future tests.

Future work:

While significant progress has been made, several challenges remain. Further optimization of welding processes, particularly for thicker weldments, is necessary to address issues such as cracking, weld process instability around open gap root pass welding and need for corrective welding. Continued thermo-mechanical modeling and mechanical characterization will be essential to refine the welding parameters and ensure the reliability and performance of the welds. The foundational data and methodologies developed in this program will serve as a basis for future qualification testing and the implementation of welded cast iron components in large-scale applications.